Cross-feeding affects the target of resistance evolution to an antifungal drug

Short title: Cross-feeding and antifungal resistance evolution

Romain Durand[1,2,3,4,5], Jordan Jalbert-Ross[1,2,3,4,6], Anna Fijarczyk[1,2,3,4,5], Alexandre K. Dubé[1,2,3,4,5], Christian R. Landry[1,2,3,4,5]

1. Département de Biochimie, de Microbiologie et de Bio-informatique, Faculté des Sciences et de Génie, Université Laval, G1V 0A6, Canada
2. Institut de Biologie Intégrative et des Systèmes (IBIS), Université Laval, G1V 0A6, Canada
3. PROTEO, Le regroupement québécois de recherche sur la fonction, l'ingénierie et les applications des protéines, Université Laval, G1V 0A6, Canada
4. Centre de Recherche sur les Données Massives (CRDM), Université Laval, G1V 0A6, Canada
5. Département de Biologie, Faculté des Sciences et de Génie, Université Laval, G1V 0A6, Canada
6. Current address: Département de Biochimie et médecine moléculaire, Faculté de Médecine, Université de Montréal, H3C 3J7, Canada

Authors for correspondence: romain.durand.1@ulaval.ca or christian.landry@bio.ulaval.ca

Abstract

Pathogenic fungi are a cause of growing concern. Developing an efficient and safe antifungal is challenging because of the similar biological properties of fungal and host cells. Consequently, there is an urgent need to better understand the mechanisms underlying antifungal resistance to prolong the efficacy of current molecules. A major step in this direction would be to be able to predict or even prevent the acquisition of resistance. We leverage the power of experimental evolution to quantify the diversity of paths to resistance to the antifungal 5-fluorocytosine (5-FC), commercially known as flucytosine. We generated hundreds of independent 5-FC resistant mutants derived from two genetic backgrounds from wild isolates of *Saccharomyces cerevisiae*. Through automated pin-spotting, whole-genome and amplicon sequencing, we identified the most likely causes of resistance for most strains. Approximately a third of all resistant mutants evolved resistance through a pleiotropic drug response, a potentially novel mechanism in response to 5-FC, marked by cross-resistance to fluconazole. These cross-resistant mutants are characterized by a loss of respiration and a strong tradeoff in drug-free media. For the majority of the remaining two thirds, resistance was acquired through loss-of-function mutations in *FUR1*, which encodes an important enzyme in the metabolism of 5-FC. We describe conditions in which mutations affecting this particular step of the metabolic pathway are favored over known resistance mutations affecting a step upstream, such as the well-known target cytosine deaminase encoded by *FCY1*. This observation suggests that ecological interactions may dictate the identity of resistance hotspots.

Author summary

Determining the paths evolution takes to make microbes resistant to antimicrobials is key to drug stewardship. Flucytosine is one of the oldest antifungals available. It is often used to treat cryptococcal infections. However, despite decades of use in the clinic, some details of its metabolism and of the mechanisms of resistance evolution still elude us. Flucytosine resistance is most often acquired specifically by inactivating a gene essential for the activation of this prodrug. We show that among many paths possible, one is overrepresented and involves a diversity of mutations that prevent enzyme expression or its activity. This path is preferred because these mutations also protect from the activation of the prodrug by non-mutant cells. A second, less frequent path to resistance, putatively involves a generalized response, which leads to fungal cells having an increased efflux capacity. The same mutants end up being resistant to the distinct and most widely used antifungal fluconazole. Our results show that the paths followed by evolution are influenced by microecological conditions and that resistance to unrelated drugs can emerge from the same mutations.

Introduction

The past decades have seen great advances in the medical field, with the death rate from complications of medical and surgical care steadily declining [1]. Numbers have also gone down for some of the leading causes of death globally, notably deaths from HIV, which have decreased by 51% between 2000 and 2019 [2]. Unfortunately, some of the treatments which help increase life expectancy also lower immune defenses, which puts patients at risk of potentially life-threatening infections caused by opportunistic pathogens [3–5]. Among them, *Candida auris*, several *Candida* species and *Aspergillus fumigatus*, all drug-resistant fungal pathogens, feature on the CDC's list of antimicrobial resistance threats [6]. Among other factors, the biological similarities between fungal and host cells make it difficult to design efficient antifungals with low toxicity [7]. Consequently, there are only five main classes of antifungals [7]. One may wonder what makes a 'good' antifungal target.

The role of most antifungals is to prevent proper synthesis of the membrane or cell wall, because they are made of components not found in mammalian cells (ergosterol, chitin-glucan, for example). If we were to look for other molecules, should the antifungal target an essential metabolic end product? An enzyme in a metabolic pathway? If the enzyme catalyzes an early step of a specific pathway, resistance could potentially arise through loss of function downstream, for instance when a toxic molecule is produced as a byproduct or through the conversion of a prodrug. Among the considerations for the development of powerful drugs targeting cell metabolism is the organization of cell communities *in vivo*. For instance, treatment can have drastically different outcomes depending on the microbe lifestyle, fungi in biofilms being notoriously less susceptible to antifungals [8].

Interestingly, despite the urgent need for better antifungals, the mechanisms of resistance are still poorly understood outside of the direct drug targets [3]. Particularly in the medical field, it is common practice to sequence as few as a single gene to look for 'common'

93 resistance-conferring mutations, which introduces a bias in databases such as MARDy [9].
94 In doing so, resistance is too often studied through a keyhole. Even more challenging is
95 deciphering if the mechanisms of resistance to a specific drug are general, or if they depend
96 on the genetic background or the environmental conditions in which they take place. Here,
97 we leveraged the power of experimental evolution coupled with whole-genome sequencing
98 (WGS) to capture a large number of mutations conferring resistance to 5-fluorocytosine (5-
99 FC, also known as flucytosine) using the model yeast *Saccharomyces cerevisiae*. We
100 focused on 5-FC because it is among the oldest antifungals, it is listed by the WHO as an
101 essential medicine [10], and its metabolism is documented enough that we can interpret this
102 data with respect to the adaptive mechanisms and rationalize the paths to resistance [11].
103
104 5-FC is a prodrug that is not toxic to fungi before it is metabolized [12]. Its metabolism
105 involves several steps, which ultimately lead to cell toxicity (Fig 1). First, it is imported into
106 the cell by several permeases, typically those involved in the import of exogenous
107 pyrimidines (Fcy2, Fur4, Fcy21, Fcy22) [13]. Next, 5-FC is deaminated by the cytosine
108 deaminase Fcy1 into the cytotoxic compound 5-fluorouracil (5-FU). 5-FU is a molecule
109 known outside of the field of antifungals that has been used to treat cancers for several
110 decades [14]. Its main activation relies on the addition of a phosphate group by the uracil
111 phosphoribosyltransferase Fur1. Misincorporation of fluoronucleotides into RNA and DNA,
112 as well as inhibition of the thymidylate synthase either cause growth arrest or cell death [14–
113 16]. Resistance to 5-FC is typically conferred by mutations in the genes involved in its
114 metabolism, preventing its import (*FCY2*), its conversion into 5-FU (*FCY1*) or the activation
115 of 5-FU (*FUR1*) (Fig 1). *FCY* genes were named after their phenotypes associated with
116 FluoroCYtosine resistance. Mutations in *FCY1* have regularly been reported as being
117 associated with 5-FC resistance in clinical isolates of a broad range of pathogens such as
118 *Candida albicans*, *Candida dubliniensis*, *Nakaseomyces* (*Candida*) *glabrata* and *Clavispora*
119 (*Candida*) *lusitaniae* [17–20].
120

Few alternative paths to 5-FC resistance have been shown, with some studies pointing at a putative pleiotropic drug response resulting in efflux-mediated resistance (Fig 1) [21–25]. This mechanism is far better characterized for azoles. Azole treatment typically favors the formation of *rho*^{0} mutants (also known as *petite* mutants), which are characterized by their loss of mitochondrial DNA. This results in an alleviation of repression of the transcription factors (Pdr1, Pdr3) regulating the expression of efflux pumps [26]. Some of these efflux pumps, for example Pdr5, end up overexpressed, conferring cross-resistance to several antifungals [26].

Because of the tight relationship with pyrimidine metabolism, the use of auxotrophic laboratory yeast strains to study the mechanisms of resistance may paint a distorted picture of how resistance to 5-FC and 5-FU comes to evolve outside the lab. Notably, it has been shown that the presence of uracil in the growth medium triggers a negative feedback by repressing the expression of the uracil permease Fur4 [27], potentially limiting cell entry by 5-FC. Not only does the use of specific lab strains narrow the number of detectable paths to 5-FC resistance, it also prevents the detection of potential epistatic effects. Indeed, the impact of the genetic background on the evolution of resistance is still poorly understood and has only recently become one of many interesting avenues of research in the field [28]. Finally, searching a relatively small gene space for resistance-conferring mutations often limits interpretations. With the decreasing costs of WGS, we can now hope to reach saturation, in that sequencing a larger number of mutants would not substantially increase the number of relevant mutations.

For the aforementioned reasons, we set up to generate hundreds of 5-FC resistant mutants, subjecting two wild prototrophic strains of *Saccharomyces cerevisiae* to experimental evolution in minimal medium. Their relative fitness was estimated in several conditions to test for respiration capacity, fitness cost and cross-resistance. We show that about a third of all mutants developed generalized resistance through loss of mitochondrial function. The

majority of the remaining two thirds evolved resistance to 5-FC and 5-FU. To explain their phenotype, the genomes of 276 of these mutants were analyzed by WGS. In particular, we sought out to determine if the resistance phenotype conferred by a given mutation was dependent on the genetic background, or if there were genetic interactions for a given background. For both backgrounds, virtually all sequenced mutants evolved resistance through loss-of-function mutations in the gene *FUR1*. Interestingly, none of the sequenced genomes showed any mutation in the well-known target *FCY1*, which we show is the result of negative selection imposed by the 5-FU-producing *FUR1* mutants. Ultimately, sequencing a large number of genomes also led to the identification of rare alleles most likely sufficient to confer resistance to 5-FC.

Fig 1. Pyrimidine and 5-FC import and metabolism around some of the known and potential mechanisms of resistance. 5-Fluorocytosine (5-FC), cytosine, uracil and 5-fluorouracil (5-FU) are represented as blue, dark purple, light purple and light blue beads, respectively. For clarity, only two permeases known to import pyrimidines are shown: Fcy2 and Fur4. In prototrophic yeast strains, pyrimidines can be synthesized *de novo* from amino acids such as glutamine and aspartate [29]. The steps leading to the obtention of the nucleotide precursors uridine monophosphate (UMP) and uridine diphosphate (UDP) are catalyzed by Ura3 and Ura6, respectively, in the *de novo* pathway [30,31]. Alternatively, pyrimidines can be imported from the medium [32]. Uracil can also be obtained by deamination of cytosine by Fcy1 [33]. Finally, UMP can be obtained by the addition of a phosphate group by Fur1 [34]. 5-FC is a prodrug, which is metabolized the same way cytosine is, except its deamination leads to the obtention of the cytotoxic compound 5-FU [35]. Based on work done in laboratory strains or other fungal species, resistance to 5-FC can arise when either of the following three steps are compromised: import, conversion and activation, typically through mutations inactivating Fcy2 (for example), Fcy1 and Fur1, respectively [36]. We also hypothesize an alternative path to resistance in the pleiotropic drug response, wherein loss of mitochondrial function leads to derepression of the

177 transcription factor Pdr3, which in turn overexpresses efflux pumps such as Pdr5. Figure
178 created with BioRender, using the structures of Fcy1 (1P6O), Fur1 from *C. albicans* (7RH8),
179 Ura3 (3GDL), Ura6 (1UKZ) and Pdr5 (7P04) and AlphaFold predictions of Fcy2 (P17064)
180 and Fur4 (P05316) [37,38].

Results

Mutants evolved in 5-FC develop cross-resistance to 5-FU

Two environmental strains of *S. cerevisiae*, LL13-040 and NC-02 were subjected to parallel experimental evolution, which generated 682 5-FC resistant mutants. All candidate resistant strains were streaked and spotted on YPG agar medium to evaluate mitochondrial function. *rho*$^-$ mutants amounted to 83/296 (28 %) and 140/386 (36 %) for LL13-040 and NC-02, respectively. The fitness of 408 5-FC resistant mutants was estimated by measuring colony growth through time on solid media.

For both backgrounds, most mutants show an expected increase in relative fitness (relative to the parental strain) in minimal medium supplemented with 5-FC compared to control conditions (rich or minimal medium) (Fig 2). *rho*$^-$ mutants show a lower relative fitness in drug-free media, with LL13-040 *rho*$^-$ mutants displaying a larger fitness defect than NC-02 counterparts. For both backgrounds, the relative fitness in minimal medium, the same medium in which the strains were evolved, is generally lower or equivalent to that of the parental strains. Additionally, when we performed the evolution experiment in the absence of 5-FC, no resistant mutant was generated. Both observations suggest that, if mutants evolved to grow better in minimal medium, none of the evolutionary routes coincidentally conferred resistance to the antifungal. We also measured the growth on minimal medium supplemented with 5-FU, the converted form of 5-FC obtained by Fcy1-mediated deamination in the pyrimidine salvage pathway (Fig 1). *rho*$^-$ and *rho*$^+$ mutants show a similar relative fitness, which is about twice that of the parental strains in minimal medium supplemented with either 5-FC or 5-FU. Interestingly, the relative fitness in 5-FC significantly correlates with the one in 5-FU, hinting at a mechanism of resistance that would take place downstream of the conversion of 5-FC into 5-FU or that affects intake of these molecules.

We hypothesized this mechanism to be either the pleiotropic drug response in the case of *rho*$^-$ mutants, or the inactivation of *FUR1* in the case of *rho*$^+$ mutants.

Fig 2. Growth of individual mutants relative to the parental strains in various media. Relative growth corresponds to the mean area under the curve (AUC, calculated on 22 h) from four replicate colonies, normalized by the WT for individual strains arrayed on solid media: YPD, SD, SD + 25 µg/mL 5-FC and SD + 6.25 µg/mL 5-FU. A two-way ANOVA followed by Tukey's multiple comparison test was performed to compare the relative fitness of *rho*$^+$ mutants to that of *rho*$^-$ mutants for each background in each condition. Statistical significance is as follows: ****, adj. *p*-value < 0.0001; ***, adj. *p*-value < 0.001; *, adj. *p*-value < 0.05; ns, not significant. Insets show the correlation between relative fitness in SD + 5-FC and relative fitness in SD + 5-FU, with the corresponding Spearman's rank correlation coefficient (S. *rho*) and *p*-value.

rho$^-$ mutants are cross-resistant to fluconazole

To test if loss of respiration induces a pleiotropic drug response, we first evaluated the fitness of *rho*$^-$ mutants in rich medium, as well as in minimal medium, supplemented or not with several antifungals belonging to distinct classes. We tested growth in the presence of three other classes of clinical antifungals: echinocandins (micafungin and caspofungin), polyene (nystatin) and azole (fluconazole). Because of the slow growth of *rho*$^-$ mutants in some antifungal conditions, we incubated the plates at 37°C. In these conditions, *rho*$^-$ mutants display a higher relative fitness in 5-FC than *rho*$^+$ mutants, while still showing a fitness defect in control media (Fig 3A). Interestingly, *rho*$^-$ mutants of both backgrounds show cross-resistance to fluconazole, with a relative growth more than twice that of the parental strain for NC-02 (Fig 3A). Also noteworthy is their fitness in micafungin, although this is likely the result of a very low growth rate (Supp Fig 1).

Since the loss of mitochondrial function in *rho*$^-$ mutants has been shown to lead to generalized resistance, we hypothesized that cross-resistance to 5-FC and fluconazole results from an increased expression or activity of efflux pumps. To test this hypothesis, we performed a rhodamine retention assay. Rhodamine is a known substrate of ABC transporters and its accumulation in cells has been shown to be inversely correlated with efflux capacity [39]. We find that virtually all *rho*$^-$ mutants display a lower count of rhodamine-fluorescent cells compared to their parental strain, confirming they have gained an increased efflux capacity (Fig 3B). Notably, both parental strains accumulate much less rhodamine than a laboratory strain deleted for all ABC transporters, meaning that parental strains were already capable of rhodamine efflux in the conditions of the experiment. Even though the NC-02 strain appears to have a diminished efflux capacity compared to the LL13-040 strain, the *rho*$^-$ mutants of both backgrounds display comparable rhodamine accumulation levels (Fig 3B). Therefore, the net gain of efflux capacity for NC-02 mutants is higher than that of LL13-040 counterparts. This efflux capacity is correlated with the measured growth in fluconazole, however the correlation is statistically significant only for NC-02 (Fig 3C). For both backgrounds, the correlation with the measured growth in 5-FC is not significant (Fig 3D). This could be explained by a lack of statistical power, but in all likelihood, a complex regulation drives the expression of multiple transporters involved in resistance to fluconazole, as well as 5-FC. Another potential mechanism is that resistance to 5-FC could be binary, whereby enough efflux above a threshold would confer resistance, whereas it would be gradual for fluconazole, creating a correlation between efflux and growth.

Fig 3. Cross-resistance of *rho*$^-$ mutants to 5-FC and fluconazole may be explained by efflux capacity. A) Relative growth corresponds to the mean area under the curve (AUC, calculated for the first 22 h of incubation) from four replicate colonies, normalized by the WT for individual strains arrayed on solid media: YPD, SD, SD + 25 µg/mL 5-FC, SD + 0.5 µg/mL micafungin, SD + 2 µg/mL caspofungin, SD + 16 µg/mL nystatin and SD + 64 µg/mL fluconazole. A two-way ANOVA followed by Tukey's multiple comparison test was performed

to compare the relative fitness of *rho*$^+$ mutants to that of *rho*$^-$ mutants for each background in each condition. Statistical significance is as follows: ****, adj. *p*-value < 0.0001; ***, adj. *p*-value < 0.001; *, adj. *p*-value < 0.05; ns, not significant. B) Rhodamine retention assay. Blue bars indicate the resulting detection thresholds (one negative control for each background i.e. cells not treated with rhodamine). *abc*Δ (s_012 in Supp Data 1) was used as the positive control. C, D) Rhodamine retention (data from panel B normalized with the WT) and relative growth in C) fluconazole or D) 5-FC (data from panel A) are compared, with the corresponding Spearman's rank correlation coefficient (S. *rho*) and *p*-value.

rho$^+$ mutants display a large number of distinct loss-of-function mutations in *FUR1*

Next, we focused on the mechanisms of resistance at play in *rho*$^+$ mutants. To make sure we identified resistance conferring mutations, including potentially rare ones, we sequenced the genomes of most assayed *rho*$^+$ mutants (149/160 LL13-040 mutants and 127/134 NC-02 mutants). Overall average sequencing coverage was around 60X, with no apparent CNVs (Supp Fig 2). Two computational methods were carried out to detect indels and SNPs, one with stringent criteria ("samtools"), and one with more tolerant criteria ("gatk"). Because of the frequency of mutations observed in *FUR1* in our preliminary analysis, we also directly amplified and Sanger sequenced *FUR1* (including the promoter region) from the same genomic DNA for most of these mutants. We included WT controls as well as *fcy1*Δ and *fcy2*Δ mutants for all three analyses (samtools, gatk and Sanger).

Supporting our hypothesis, most sequenced genomes (258 out of 276 mutants) harbored a mutation in *FUR1* (Fig 4A).

Fig 4. **Genome sequences analysis and validation**. A) Upset plots showing the number of unique mutated genes (# genes) detected by gatk, samtools or both for each background.

Categorical plots on top show the number of distinct genomes for which at least one variant was detected in a given gene (one dot per gene, colored according to the number of distinct mutations which have been detected). B) Distribution of the number of genes with variants per genome (as detected either by gatk or samtools) for each background. C) Data from Fig 2, where dots are colored by the mutated/deleted gene most likely to confer resistance. D) Growth assay in liquid medium for 35 resistant mutants for which a variant in *FUR1* was detected. Cultures were inoculated in SD with or without 100 µg/mL 5-FC. Relative growth corresponds to the mean area under the curve from two replicates (AUC, calculated on 46h) normalized by the WT.

Aggregating results from samtools, gatk and Sanger sequencing, we identified 118 distinct SNPs or indels in *FUR1* (Supp Data 2). The use of two computational methods to call variants proved relevant, since part of the variants were detected by only one method (Fig 4A). As expected, gatk, with its set of more permissive criteria, detected variants in around 500 genes in each background, whereas samtools detected variants in only 150 genes on average (Fig 4A). Variants in other genes than *FUR1* were rarely detected by both computational methods, which might be linked to the quality of their call (Fig 4A). Overall, approximately 120 genes per individual genome were found to have variants by either method (Fig 4B). This large number is a result of the filtering criteria, which were set to be more flexible to make sure rare mutations would not be discarded. Ultimately, the number of unique variants found in a given gene appeared as a good indicator to sort through the noise. Specifically, the number of unique variants found in *FUR1* was much larger than in any other gene, which is strong evidence that *FUR1* constitutes a hotspot for 5-FC resistance-conferring mutations (Fig 4A).

Out of all strains for which *FUR1* was Sanger sequenced (n=268), all six controls (parental strains, *fcy1*Δ and *fcy2*Δ mutants) and only 13 mutants carried the WT allele of *FUR1*. Through a detailed look into our dataset, we found three candidate target genes which could

314 alone explain the resistance phenotype of these 13 strains carrying a WT *FUR1* sequence:
315 *URA6*, *GFA1* and *ARG2*. Two LL13-040 strains and one NC-02 strain carried a background-
316 specific mutation in *URA6*: R52S for the former, G73S for the latter. Eight NC-02 strains
317 carried one of four mutations in *GFA1*: V478F, G482R, G492S and N496K. One NC-02
318 strain carried a K113* mutation in *ARG2*. Interestingly, the corresponding mutants display a
319 relative fitness distinct to that of *FUR1* mutants (Fig 4C and Supp Data 3). Notably, the
320 mutations detected in *URA6* and *GFA1* are harbored by strains resistant to 5-FU, whereas
321 the *ARG2* mutant is only mildly resistant to 5-FC in our experimental conditions (Fig 4C). All
322 identified mutations in these three genes (n=7) are predicted by mutfunc (see methods
323 section) to impact conserved residues with five out of seven also predicted to impact protein
324 stability. Their effect is therefore likely to be through loss of function.
325
326 Among the sequenced strains for which no clear candidate resistance mutation was
327 identified, one appears to have been initially miscategorized as resistant to 5-FC, four
328 display the same relative fitness in 5-FC and 5-FU as *FUR1* mutants (and are therefore likely
329 *FUR1* mutants as well) and one appears to be mildly resistant to 5-FC but not 5-FU (Fig 4C).
330 Finally, most unsequenced *rho*$^{+}$ mutants showed little to no resistance, which suggests they
331 were false positives of the evolution experiment (Fig 4C).
332
333 To further investigate the extent and potential mechanisms of resistance, 35 resistant
334 isolates (across both backgrounds) for which mutations were predicted in *FUR1* were tested
335 in a growth assay, alongside the parental strains, and the deletion mutants for *FCY1*, *FCY2*
336 and *FUR1* (s_004/5/6/9/10/11 in Supp Data 1). All tested mutants showed a relative fitness
337 similar to their null mutant counterpart (Fig 4D). This suggests most mutations inactivate the
338 function of *FUR1* and are sufficient to explain the resistance phenotypes, meaning that
339 mutations in other genes likely play no role (Fig 4C). Importantly, the relative fitness of the
340 *fcy1*Δ mutants was comparable to that of all tested *FUR1* mutants. The reason why
341 inactivating mutations in *FCY1* were not picked up in our experiment is thus not because

they provide lower resistance levels than *FUR1* inactivating mutations in these conditions (see below).

Most mutations identified in *FUR1* were confirmed by our three detection methods (samtools not picking up indels), with all samples sequenced by Sanger (268 out of 282 samples sequenced by WGS) confirming what had been detected by WGS (Fig 5A). One mutation (R110G) stands out as being much more prevalent than others in LL13-040 genomes (Fig 5A). Further examination confirmed that it is shared among 39 strains which arose from the same preculture (Supp Fig 3). This could be explained by a rapid fixation of the mutation that was segregating in the preculture. It is important to note however that it constitutes a rare case, since we often selected less than 20 mutants per preculture, which generally carried different mutations each (Supp Fig 3).

To understand why all validation mutants behaved like the null mutant, we compared their predicted impact to that of all possible substitutions. Out of 4,104 possible missense mutations in Fur1, 1,279 are predicted to impact stability. Our dataset captured a total of 76 missense mutations, 42 of which are predicted to impact stability. This is significantly more than what can be expected by chance (Fisher's exact test *p*-value = 1.39e-5, Supp Fig 4A). The same observation can be made of mutations predicted to impact function based on conservation, with 67 out of 2,667 being captured in our dataset (Fisher's exact test *p*-value = 4.96e-6, Supp Fig 4B). The results are consistent with loss-of-function mutations. We find that the substitutions in our dataset are predicted to destabilize Fur1 with generally high ΔΔG values, with no apparent bias in terms of position along the sequence (Supp Fig 4A and Supp Fig 5). Expression of *FUR1* from a centromeric plasmid under its native promoter restored sensitivity in most tested mutants (n=32), including all with a mutation introducing a stop codon, confirming the detected mutations lead to loss of function (Fig 5B). Interestingly, some mutations could only be partially complemented, with four strains growing at more than 75% the rate of their corresponding control (vector with no expressed ORF, Fig 5B). To

better understand this dominant negative effect, all residues for which we detected a mutation in our dataset were mapped on the predicted structure of the Fur1 tetramer from *C. albicans* (PDB: 7RH8). We find that most mutated residues are not located close to the active site, but instead appear to be involved in structurally important folds and helices (Fig 5C). Additionally, some mutated residues reside at the interface between two chains, which could indicate that the mutation prevents proper assembly of the tetramer (Fig 5C). Namely, G104 and G205 appear to interact each with a cysteine residue from the adjacent chain (Fig 5C insets). This observation could also explain why the mutations G104D and G205W cannot be complemented with the WT allele of *FUR1* as they could also perturb the assembly of tetramers that would include WT chains.

Fig 5. Mutations observed in Fur1 lead to loss of function. (A) Upset plots showing the number of unique mutations identified in Fur1 for each background. Categorical plots on top show the number of distinct genomes for which the same mutation was detected. Only one amino acid change resulted from two adjacent mutations (back-to-back in the same codon), all others corresponding to a single SNP or indel. B) Growth assay for 32 out of 35 resistant mutants tested in Fig 4D, with pMoBY expressing or not *FUR1* from its native promoter. Relative growth corresponds to the area under the curve calculated on 25 h for the mutant with pMoBY-*FUR1* divided by the same parameter for the mutant with pMoBY. Mutants were grown from single colonies in SD + 100 µg/mL 5-FC (+ G418 to maintain pMoBY). Colored dots indicate the same mutation was detected in the mutants from both backgrounds. Two mutations for which expression of the WT allele of *FUR1* did not restore 5-FC sensitivity are highlighted. A closer look at the residues in the next panel suggests a putative role in assembly of the tetramer. C) Location of substitutions from our dataset on the predicted structure of Fur1, visualized using UCSF ChimeraX [40]. The tetramer (*C. albicans* Fur1 assembly 7RH8) is represented in light gray, with 1 chain in dark gray. Residues found to be mutated at least once in our dataset are colored in pink. UTP molecules are represented in sticks colored by atom. Two insets zoom in on one interface each (the slightly opaque one

398 depicts the interface at the back of the represented structure). The highlighted residues
399 (each one from a different monomer) appear to interact with one another to ensure proper
400 assembly of the tetramer.

401 *FUR1* path to resistance prevents selection of *FCY1* mutations

402 One of the known resistance genes to 5-FC encodes for the cytosine deaminase Fcy1,
403 which acts upstream of Fur1 in the pyrimidine salvage pathway (Fig 1). We included *fcy1*Δ
404 mutants in our validation experiments as positive controls. However, we were surprised to
405 find no single Fcy1 mutants in our set of sequenced genomes. As loss of function in *FCY1* is
406 sufficient to lead to resistance and many mutations in the gene are destabilizing enough to
407 cause resistance [41], one would expect *FCY1* mutations to also be frequent in our
408 experiments.
409
410 To validate the absence of detectable mutations in *FCY1*, we randomly selected mutants
411 (n=14) and performed Sanger sequencing: all carried the wild-type sequence. Next, we
412 confirmed that *FCY1* is well expressed in LL13-040, using a mEGFP protein fusion (Supp
413 Fig 6A). Finally, we evaluated the functionality of Fcy1 in parental strains. A growth assay
414 using cytosine as the sole nitrogen source in minimal medium confirmed that both strains
415 can grow, which would not be possible without the deamination of cytosine performed by
416 Fcy1 (Supp Fig 6B).
417
418 Next, we sought out to confirm the fitness of the *fcy1*Δ mutants in liquid medium compared
419 to our 5-FC mutants as a lower fitness could explain why they were not picked up in our
420 experiments. We performed growth assays to calculate the relative fitness in three
421 conditions with minimal medium: with or without 5-FC and one condition where the only
422 nitrogen source is cytosine. As expected, the *fcy1*Δ mutants fared well compared to our
423 evolved mutants in 5-FC but displayed the lowest relative fitness among *rho*$^{+}$ mutants in

cytosine (Supp Fig 7A). In comparison, virtually all *rho*$^{+}$ mutants have little to no fitness tradeoff in cytosine, indicating that *FCY1* is functional.

Interestingly, when we compared the relative fitness measured in liquid medium versus the one measured on solid medium, we observed that the *fcy1*Δ mutant shows a significant fitness defect on solid medium when grown alongside other mutants (Supp Fig 7B). A recent study by our group showed that *fcy1*Δ could grow on plates supplemented with cytosine as the only nitrogen source as long as strains with a functional *FCY1* allele (*FCY1*$^{+}$) were growing in proximity [41]. The auxotrophy of a *fcy1*Δ strain can therefore be rescued by cross-feeding uracil from *FCY1*$^{+}$ strains. We hypothesized that this could also occur for 5-FU and, through interactions between cells of different genotypes and diffusion in the medium, it would lead to strains with a loss of function of *FUR1* (*fur1*$^{-}$ strains) taking over strains with a loss of function of *FCY1* (*fcy1*$^{-}$ strains) during experimental evolution.

Specifically, if a mutant is sensitive to a compound effluxed by its neighbor, its growth will be inhibited. The ultimate toxic compound produced from the prodrug is 5-FUMP, downstream of Fcy1 and Fur1. This means that in a complex community, a *FCY1*$^{+}$ strain could produce 5-FU, which would inhibit its growth and that of *fcy1*$^{-}$ neighboring cells too, provided they are *FUR1*$^{+}$ (Fig 6A). On the other hand, a *fur1*$^{-}$ strain would be resistant to its own production of 5-FU and to that of neighboring *FCY1*$^{+}$ cells (Fig 6A). During experimental evolution, both *fcy1*$^{-}$ and *fur1*$^{-}$ mutants could occur but because they do so at low frequency at first, only the latter would increase in frequency. Pure cultures of *fcy1*$^{-}$ and *fur1*$^{-}$ would however be both equally resistant to 5-FC, as our previous results revealed. If this model is correct, conditioning the medium with a *fcy1*Δ strain should allow growth of a *fur1*Δ strain, whereas the opposite would lead to growth inhibition. We confirmed this prediction (Fig 6B). For both backgrounds, conditioning the medium with the *fcy1*Δ mutant led to the *fur1*Δ mutant growing significantly better than the WT. On the other hand, conditioning the medium with the *fur1*Δ mutant led to growth inhibition of both the WT and the *fcy1*Δ mutant.

Fig 6. *FCY1*-mediated resistance is context-dependent. A) Predicted cross-feeding interactions between cells with different alleles of *FCY1* and *FUR1*. Uracil (top) and 5-FU (middle) are expected to diffuse in the medium and be converted by Fur1 of neighboring cells, which would allow or inhibit growth, respectively. Notably, the growth of any *FUR1*$^{+}$ cells, regardless of their *FCY1* allele, will be inhibited because of 5-FU cross-feeding. On the contrary, any *fur1*$^{-}$ cells would grow despite 5-FU cross-feeding (bottom). Figure created with BioRender, using the structures of Fcy1 (1P6O) and Fur1 from *C. albicans* (7RH8). B) Medium conditioning assay. First, cultures of the deletion mutants were prepared in SD with or without 1.56 µg/mL 5-FC. After reaching an OD_{600} of 0.6, the cultures were filtered and the medium was transferred to a 96-well plate. Cultures were inoculated with either the WT or the other deletion mutant. Relative growth corresponds to the area under the curve (AUC) normalized by the WT and was obtained from biological triplicates. A two-way ANOVA followed by Tukey's multiple comparison test was performed to compare the relative growth in SD with 5-FC to the one obtained in SD without 5-FC in each condition. Statistical significance is as follows: ****, adj. *p*-value < 0.0001; ns, not significant. C) Competition assay. Individual cultures of the deletion mutants were prepared in SD without selective pressure, then pooled in equal volumes, serially diluted and plated on large petri dishes containing SD with 1.56 µg/mL 5-FC. For each counted colony, the genotype (*fcy1*Δ or *fur1*Δ) was confirmed by PCR. For each background, the relationship between CFU count of either mutant and the inoculum concentration was assessed by a Chi-square test of independence, performed on the cumulative sum of counts obtained from two independent experiments. D) Inhibition assay. For each background, a culture of the *fcy1*Δ mutant was inoculated in SD 1.7% agar with or without 25 µg/mL 5-FC and poured on top of thin 2% agar plates containing the matching medium. A culture of the *fur1*Δ mutant was then spotted on top. Uncropped pictures are provided in Supp Fig 8.

In this assay we show the ultimate outcome of applying selective pressure to both mutants, but what happens if the only source of 5-FC comes from the solid medium on which the population is plated? To evaluate such a scenario, we designed a competition experiment, in which both mutants are grown individually with no selective pressure. For each background, the *fcy1*Δ is pooled with the *fur1*Δ culture. Serial dilutions are then plated on large petri dishes with 5-FC, and mutants are identified by multiplexed colony PCR. We show that the survival of *fcy1*Δ mutants significantly depends on the inoculum concentration (Fig 6C). Specifically, if a 1:1 mix of *fcy1*Δ and *fur1*Δ mutants is plated at 10^{-5} OD_{600}, the same ratio will be observed for the growing colonies. However, when the same mix is plated at a concentration 100 times higher, all tested colonies are *fur1*Δ, meaning *fcy1*Δ cells are killed by 5-FU cross-feeding. To further confirm the link between cell density and cross-feeding, we performed an inhibition assay, where a culture of the *fur1*Δ mutant is spotted on a *fcy1*Δ lawn spread on medium with 5-FC. For both backgrounds, we were able to see a clear inhibition zone around the *fur1*Δ spot (Fig 6D).

In summary, the design of our experimental evolution, where the mutants are selected by spotting precultures on a plate, negatively selects against spontaneous *FCY1* mutants. This would likely occur as well in a mixed community.

Discussion

Efflux-mediated resistance to 5-FC in *rho*$^-$ mutants

We generated and analyzed the fitness of hundreds of independent 5-FC resistant mutants to identify the most frequent molecular signatures of resistance to this antifungal. Challenging a common assumption of the usual paths to 5-FC resistance, we show that around a third of mutants gained resistance through a previously unknown mechanism likely involving drug efflux rather than inactivation of key metabolic enzymes. This path to resistance, often referred to as a pleiotropic drug response, is well characterized for azole resistance [42–44]. Mutants which have lost mitochondrial function are no longer able to respirate and display a specific *petite* morphotype on glucose-containing medium. Resistance in this case therefore comes with a tremendous tradeoff. In turn, they display enhanced efflux activity, which confers generalized resistance. To date, this resistance mechanism has not been described for 5-FC.

Here, we confirm that 5-FC treatment at least selects for *rho*$^-$ mutants, which are cross-resistant to 5-FC and fluconazole (Fig 3A). However, we find no significant correlation between rhodamine accumulation, indicative of increased efflux capacity through ABC transporters, and fitness in 5-FC (Fig 3D). This corroborates previous observations that 5-FC treatment, while selecting for rho^0 mutants, does not affect the expression of transcription factors such as Pdr1 or the related expression of ABC transporters [22]. On the other hand, we do observe a significant correlation between rhodamine accumulation and fitness in fluconazole for NC-02 mutants (Fig 3C). Since azole resistance has also been associated with MFS transporters [45], one possible explanation for the discrepancy would be that a mechanism overlapping both regulatory pathways is sufficient to confer resistance to both classes of antifungals. One study supporting this hypothesis reported that a substitution in

522 the gene *MRR1* was sufficient to confer cross-resistance to 5-FC and azoles in clinical
523 isolates of *C. lusitaniae* [25]. This gene encodes a transcriptional regulator, which when
524 mutated upregulates the expression of the multidrug transporter encoding gene *MFS7*.
525 Another study reported reduced susceptibility to azoles in 5-FC resistant isolates of several
526 pathogenic fungi, including *C. albicans* [46].
527
528 Although future work is needed to uncover the exact mechanisms governing 5-FC resistance
529 through efflux, it is plausible that pathogenic fungi could evolve along this path, in addition to
530 the more commonly described resistance paths in the canonical pathway. Losing
531 mitochondrial function would be unfavored in environments that require respiration, given the
532 strong fitness cost in drug-free conditions. However prolonged treatments could render that
533 evolutionary path more accessible, as suggested by reports of such selection in a clinical
534 isolate of *N. glabrata* in response to fluconazole [47].

535 *FUR1*-inactivating mutations confer 5-FC resistance in *rho*$^+$ 536 mutants

537 Using WGS, we found that most *rho*$^+$ mutants gained resistance through *FUR1* inactivation.
538 Interestingly, a large diversity of mutations was detected in this gene. In contrast, the
539 MARDy database only lists two *FUR1* mutations conferring resistance to 5-FC at the time of
540 writing (version 1.1DB:1.3WS, http://mardy.dide.ic.ac.uk/). Despite the low number of
541 reported mutations (including the ones reported in other studies but not listed in MARDy
542 [11]), our experiment still recapitulates some of them. Most importantly, they correspond to
543 mutations of clinical relevance, such as F211I and G190D found in clinical isolates of *C.*
544 *auris* and *N. glabrata*, respectively [48,49]. Our work shows that the available paths through
545 mutations in *FUR1* are far more diverse than the literature lets appear. Most mutations in
546 *FUR1* appear to be loss-of-function mutations. We observed several indels (deletions and
547 insertions of up to 49 and 39 bp, respectively) and five mutations affecting the translation

start site of Fur1 (M1V, M1I, M1L, M1K, M1T) (Supp Data 2). Many more are predicted to impact the stability of the protein. This would make resistance through mutations in *FUR1* very likely since many of the possible amino acid changes are predicted to impact the stability of Fur1 and/or conserved regions (Supp Fig 4), in addition to all possible stop codons and other possible frameshifting indels. Not only the mutations picked up in our experiments capture both of these phenomena (Supp Fig 4), some also appear to likely affect proper assembly of the Fur1 tetramer (Fig 5C).

It is also possible that the drug concentration used to select for resistant mutants was high enough that a partially functional Fur1 would not confer resistance. It would be interesting to study the relationship between the extent of Fur1 inactivation and inhibitory concentrations to formally test this hypothesis. In any case, our results strongly suggest that the number of resistance-conferring mutations in fungal pathogens is profoundly underestimated. They do confirm however that resistance can emerge rapidly in response to 5-FC monotherapy [50]. That being said, rapid emergence of resistance does not seem to be specific to 5-FC, whether it is observed through experimental evolution or in the clinic. For example, cases have been reported where resistance through nonsense mutations in *FUR1* was rapidly acquired upon combination therapy with caspofungin [51]. Cross-resistance to fluconazole (and potentially other azoles) has also been reported to evolve rapidly in clinical settings [46]. The same can be said of nystatin resistance in experimental evolution [52]. Additionally, the fact that resistance to different antifungals is connected through shared resistance mutations despite their apparent lack of similarity in their mode of action is worrisome and stresses the need for more studies on cross-resistance.

Alternative paths to resistance in *rho*$^{+}$ mutants

Our experiment led to the identification of three other genes potentially conferring resistance to 5-FC when mutated: *URA6*, *GFA1* and *ARG2* (Fig 4C).

URA6 encodes the enzyme which catalyzes the step right after the reaction performed by Fur1 (Fig 1), therefore it is highly likely that the detected mutations inactivate *URA6* and are sufficient to confer 5-FC and 5-FU resistance. A temperature-sensitive mutant of this enzyme in a laboratory strain is known to be resistant to 5-FU, confirming that loss of function is responsible for resistance [31]. *GFA1* encodes an important enzyme involved in the biosynthesis of chitin. Some studies have shown fungal cells can display increased chitin levels in response to fluconazole or echinocandins [53–55], however it appears to be one of many consequences of a generalized stress response. Both *URA6* and *GFA1* are essential in auxotrophic laboratory strains [31,56]. This shows that epistasis can play an important role in the evolution of resistance, and that the use of prototrophic strains in experimental evolution experiments will likely lead to different outcomes.

Finally, it has previously been shown that deletion of *ARG2* can confer resistance to 5-FU, through crosstalks between the ornithine biosynthesis pathway and the pyrimidine biosynthetic pathway [57]. The hypothesized mechanism is that blocking ornithine formation hinders the consumption of carbamoyl-phosphate, both being required for the synthesis of arginine. As a result, carbamoyl-phosphate is used as an early precursor of UTP, which ends up being produced in larger quantities than 5-FUTP [57]. This would corroborate a previous observation that five other genes involved in arginine metabolism are linked with 5-FC resistance [23].

Our results highlight the need for studies using prototrophic strains, instead of the popular laboratory strains, as they allow the identification of rare alleles conferring resistance.

FUR1 is the main target to confer 5-FC resistance

Out of all genes involved in the metabolism of 5-FC, we unexpectedly detected mutations only in *FUR1* and *URA6* (Fig 4C). Resistance to 5-FC in clinically relevant fungi typically results from mutations in *FCY2*, *FCY1* and/or *FUR1* [17,58,59]. Since resistance often requires loss of function of those genes, redundant entry routes in *S. cerevisiae* can explain the absence of resistance mutations in genes involved in the import of 5-FC, namely *FCY2*, *FCY21*, *FCY22* and *FUR4* [13] as their loss of function would be masked by others. The case of *FCY1* was more difficult to interpret as there is no known redundancy for its function. We hypothesized that depending on the context, *FUR1* could be a more likely target than *FCY1* due to cross-feeding. In a mix of $FCY1^{+}$ and $fcy1^{-}$ cells, 5-FU would be produced and secreted, leading to the death of $FCY1^{+}$ cells, as well as loss-of-function mutants. The benefits of losing the cytosine deaminase function would therefore be highly specific to the ecological context.

Accordingly, we performed a growth-based experiment in which the medium was previously conditioned by the growth of either a *fcy*1Δ mutant or a *fur1*Δ mutant (Fig 6B). A medium conditioned by the latter contains 5-FC, as well as 5-FU, as a result of deamination of 5-FC by Fcy1. 5-FU being toxic for any cell that encodes a functional Fur1, it imparts selective pressure upon *FUR1* mutants. We further confirm this hypothesis by showing that plating a mix of *fcy1*Δ and *fur1*Δ mutants at high cell density prevents the growth of *fcy1*Δ cells (Fig 6C). Finally, spotting the *fur1*Δ mutant on top of a *fcy1*Δ lawn leads to the apparition of an inhibition zone, delimiting the range of diffusion of 5-FU (Fig 6D and Supp Fig 8).

Compound sharing during the selection step dilutes the populations of cells in which mutations impact any step upstream of the conversion of 5-FU. This is of the utmost ecological importance, since the ecological context will define which mutations are more likely to lead to resistance [60].

No strong background-dependent effect for path to resistance but many background-dependent effects on fitness

Even though we used two distinct environmental isolates as parental strains, we observe strong parallel evolution of resistance. Notably, the main outcome of our evolution experiment did not seem to be affected by the presence of active transposable elements in only one of the two parental strains (LL13-040). Indeed, for both backgrounds, most evolved strains gained resistance through loss-of-function mutations in *FUR1*. However, differences in fitness reflect the different behaviors of each background before and after evolution. For example, even though both parental strains grow at comparable rates in all tested conditions (Supp Fig 1), NC-02 displays more rhodamine accumulation than LL13-040 (Fig 3B). After evolution however, *rho*$^-$ strains of both backgrounds display strikingly similar distributions in rhodamine accumulation (Fig 3B). One background, NC-02, therefore evolved to gain much more efflux capacity than the other. This observation is corroborated by the significant correlation with fitness in fluconazole, which is again markedly higher for NC-02 *rho*$^-$ strains compared to LL13-040 counterparts (Fig 3C). Similarly, the same mutants show a lower fitness tradeoff in drug-free media (Figs 2 and 3A). Together, our results could indicate that NC-02 would potentially evolve along a broader range of paths to resistance. Interestingly, this hypothesis is also supported by the mutations detected in the sequenced genomes. For example, more indels were detected in *FUR1* for NC-02 strains (Fig 5A). Two genes potentially sufficient to confer resistance, *GFA1* and *ARG2*, were found to be mutated only in NC-02 strains (Fig 4C). On the other hand, a single mutation in Fur1 (R110G) was found to be present in 39 different LL13-040 strains (Supp Fig 3). And despite selection seemingly acting more strongly in one background than the other, we found an identical number of unique mutations in *FUR1* for each background (52 background-specific mutations for each background and 14 shared mutations, Supp Data 2 and Supp Fig 5).

Experimental design and evolutionary relevance

Our experimental design does not represent a real-world clinical situation in which 5-FC would be used for treatment. However, we revealed a very interesting community interaction that can affect the route of evolution. Upon treatment of an infection, rapid establishment of resistance would arguably be impacted by two main factors: the local concentration of antifungal and the local population size. The first factor determines for instance the efficiency of selection and the second the size of the mutational supply and the efficiency of selection. Our results indicate that population size or density could also affect the route of evolution.

Drug concentration is rarely homogeneous, but instead exists as a spatiotemporal gradient linked to the inherent pharmacodynamic properties of the drug, such as imperfect drug penetration [61]. This can have a crucial effect on the establishment of resistance. For example, it can allow (or not) the expansion of a resistance-conferring mutation from a single cell to a whole subpopulation [62]. Drug concentration has also been shown to impact the nature of beneficial mutations and affect whether a population will develop resistance or tolerance [63]. Local population size is also heterogeneous. For example, a localized higher density of cells could be the result of a biofilm having developed on a catheter [8,64]. Our findings suggest that the benefits of losing either of two consecutive steps in a path, both of which confer resistance on their own, will be dictated by the local conditions and density. In conditions that allow cross-feeding and diffusion of small molecules, the loss of the initial step (Fcy1) would not be advantageous. However, for isolated cells or in conditions where the diffusion of nutrients is highly limited, it might be, hence the discrepancy in the resistance phenotype of the *fcy1*Δ mutant on a shared plate versus in an isolated well (Supp Fig 7). In comparison, the loss of the second step (Fur1) is advantageous, no matter if cells are isolated or in close contact (Fig 6C).

677 Ultimately, evolution experiments such as our study highlight relatively narrow but still very
678 relevant features of evolution of resistance. And even with the complex challenge that is the
679 accurate reproduction of clinically relevant environments, these studies still manage to
680 capture resistance mutations found in clinical isolates [44].

Materials and methods

Strains, plasmids, primers and culture media

We used two environmental strains of *S. cerevisiae*: LL13-040 [65] and NC-02 [66], both wild isolates collected from trees in North America. Unlike LL13-040, previous whole-genome analysis of NC-02 revealed no active transposable element [66], which could potentially change the types of resistance mutations the strains would have access to. For both strains, only haploids were used to be able to detect recessive mutations. First, the *HO* locus was replaced by a nourseothricin resistance marker in LL13-040 and a hygromycin resistance marker in NC-02. Strains underwent sporulation and dissection. Haploid selection and mating type were confirmed by multiplexed PCR. All subsequent experiments were performed using the corresponding haploid strains of mating type **a**. They are referred to thereafter as the "parental" strains in our experimental evolution and were found to have 0.39% nucleotide divergence (averaged across chromosomes). Strains used in this study are listed in Supp Data 1. Constructions were obtained by standard transformation from competent cells using plasmids and primers listed in Supp Data 1. The following culture media were used: YPD (1% yeast extract, 2% bio-tryptone, 2% glucose, with or without 2% agar), YPG agar (1% yeast extract, 2% bio-tryptone, 3% glycerol, 2% agar), SD (MSG) (0.174% yeast nitrogen base without amino acids, 2% glucose, 0.1% monosodium glutamate), SD (NH_4) (0.174% yeast nitrogen base without amino acids, 2% glucose, 0.5% ammonium sulfate), SC (SD with standard drop-out mix). When indicated, the following compounds were added to the medium: 5-FC (Fisher Scientific), 5-FU (Fisher Scientific), cytosine (Fisher Scientific), methylcytosine (Fisher Scientific), micafungin (Toronto Research Chemicals), caspofungin (Cedarlane Labs), nystatin (BioShop Canada), fluconazole (Cedarlane Labs), nourseothricin (Millipore Sigma), hygromycin B (BioShop Canada), G418

(BioShop Canada). Unless specified, most biochemical products were acquired from Fisher Scientific or BioShop Canada.

Experimental evolution

The evolution experiment was adapted from [67] to isolate a large number of independent 5-FC resistant mutants. Parental strains were streaked from glycerol stocks onto YPD agar medium, then incubated three days at 30°C. 10 mL YPD was inoculated with a single colony, then incubated for 24 hours at 30°C with shaking. The corresponding number of mitotic generations was calculated from measurements of cell concentrations before and after incubation using cell counts estimated by flow cytometry for four biological replicates, with a guava easyCyte HT cytometer (Cytek, blue laser): LL13-040, 5.3 ± 0.5 generations; NC-02, 5.4 ± 0.5 generations. Each 24 h preculture was used to inoculate a 96-deep-well plate with 1 mL synthetic minimal medium (SD) supplemented with 1.56 µg/mL 5-FC, at a final concentration of 0.1 OD_{600}. Border wells were filled with 1 mL sterile water to prevent evaporation. Plates were sealed with porous adhesive film and incubated for 72 hours at 30°C with shaking. Finally, cultures were spotted on SD agar plates with or without 6.25 µg/mL 5-FC to select 5-FC resistant mutants. All mutants were streaked on YPD agar medium to isolate single colonies, only one of which per mutant was selected for further experiments.

rho$^-$ (*petite*) mutants were identified by their morphotype. Once enough mutants were generated, a 96-well plate with 1 mL YPD was inoculated and incubated overnight at 30°C. The plate was then used to prepare a glycerol stock, as well as spotting on YPG agar medium to confirm *rho* status. Overall, the evolution experiment was iterated eight times, for a total of 49 precultures (26 for LL13-040 and 23 for NC-02), generating a total of 682 5-FC resistant mutants (296 LL13-040 mutants and 386 NC-02 mutants). Two more iterations without 5-FC selection were performed to evaluate whether acclimation to minimal medium

731 could be enough to acquire resistance. It was not, since neither generated any 5-FC
732 resistant mutant.
733
734 Media conditions for the evolution experiment were initially decided based on preliminary
735 growth assays using the constructed haploid LL13-040 strain. Specifically, we noted that the
736 use of minimal medium greatly increases 5-FC sensitivity, the absence of uracil being partly
737 responsible for this effect (Supp Fig 9A). The final concentration of 5-FC used in the
738 evolution experiment was chosen based on dose-response curves in SD medium obtained
739 from biological triplicates of both strains. In the conditions of this experiment (see section
740 below), a concentration of 1.56 µg/mL 5-FC corresponds to inhibition coefficients of 93.5 ±
741 0.8% and 91.8 ± 0.3% for LL13-040 and NC-02, respectively (Supp Fig 9B). In an initial
742 experimental evolution trial, this concentration yielded 15 LL13-040 spontaneous mutants,
743 compared to only 3 when using 0.78 µg/mL 5-FC. A 10% cutoff (at least six mutants out of
744 60 wells inoculated on each plate) ultimately prompted us to use 1.56 µg/mL 5-FC for all
745 iterations of the evolution experiment.

746 Automated growth measurements on solid medium

747 The growth of resistant strains, as well as parental strains and deletion mutants for *FCY1*
748 and *FCY2* was assayed with a BM3-SC robot (S&P Robotics Inc.). First, plates of mutants
749 were printed on YPD OmniTrays. Then, mutants were rearrayed depending on their *rho*
750 status. Finally, the plates were replicated onto solid medium, either rich medium, or minimal
751 medium with or without antifungal. The following sections describe in more detail the
752 protocol followed depending on the *rho* status.

753 *rho*$^+$ mutants

754 A liquid culture of strain s_009 was used to print a border on a YPD 384-array. 300 *rho*$^+$
755 mutants (including controls) were then rearrayed onto the same 384-array from five 96-array

sources. The resulting 384-array was expanded into a 1536-array to have four replicates for each mutant. The 1536-array was replicated six times to obtain the source plates for the fitness measurements. Source 1 was replicated onto five destination plates: YPD, SD, SD + 25 µg/mL 5-FC, SD + 1.56 µg/mL 5-FU, SD + 6.25 µg/mL 5-FU, which were incubated for 22 h at 30°C. Sources 2-6 were each replicated onto three destination plates for a total of 15 conditions: YPD, SD, SD + 25 µg/mL 5-FC, SD + 16/32/64 µg/mL fluconazole, SD + 4/8/16 µg/mL nystatin, SD + 0.25/1/2 µg/mL caspofungin and 0.0625/0.25/0.5 µg/mL micafungin. Plates were incubated for 90 h at 37°C. During both incubations, pictures of each plate were taken every 2 h in a spImager custom robotic platform (S&P Robotics Inc.).

rho$^-$ mutants

Similarly, two 96-arrays were prepared, one with only LL13-040 mutants, the other with only NC-02 mutants. For both, a liquid culture of the corresponding *fcy1*Δ mutant was used to print the border. 118 *rho*$^-$ mutants as well as controls were rearrayed from either three (NC-02) or four (LL13-040) 96-array sources. The two resulting 96-arrays were expanded into two 384-arrays to have four replicates for each mutant. For each background, the 384-array was replicated five times to obtain the source plates for the fitness measurements. Similar growth media conditions were tested. Additionally, both plates were replicated onto YPG arrays to confirm *rho* status. Following this quality control step, four mutants were detected as being initially misannotated as *rho*$^-$ (three LL13-040 mutants and one NC-02 mutant) and were therefore excluded from all analyses (Supp Fig 10).

Colony size analyses

Pictures were cropped, then converted into inverted gray levels using scikit-image [68]. Colony sizes were quantified using pyphe-quantify in batch mode [69]. The area parameter was used to generate growth curves and calculate the corresponding area under the curve (AUC) using the composite trapezoidal rule. For each mutant, the relative fitness was

781 calculated as the ratio of the mean AUC (absolute fitness) divided by the corresponding
782 mean AUC obtained for the WT parental strain.

783 Cytometry

784 Rhodamine accumulation assay

785 In order to evaluate the efflux capacity of *rho*$^-$ mutants, we used rhodamine 6G, a fluorescent
786 dye known to be a substrate of ABC transporters. Measurement of intracellular accumulation
787 of rhodamine was adapted from [70]. The two 96-arrays of *rho*$^-$ mutants for LL13-040 and
788 NC-02 (obtained as described above) were inoculated in 96-deep-well plates containing 1
789 mL YPD and incubated overnight with shaking at 30°C. For both plates, two controls were
790 added: the parental strain and a strain with deletions for all ABC transporters (*PDR5 SNQ2*
791 *YBT1 YCF1 YOR1*, s_012 in Supp Data 1) [71], therefore incapable of rhodamine efflux. In
792 the morning, both plates were subcultured at 0.15 OD_{600}, then incubated at 30°C with
793 shaking until they reached 0.6 OD_{600}. For this step, one of the mutants was subcultured
794 twice to later have a control without rhodamine. 200 uL was transferred to a sterile V-shaped
795 plate. Rhodamine 6G (Millipore Sigma) was added to a final concentration of 10 µg/mL
796 except for 1 well. Plates were sealed with porous adhesive film and incubated 30 min at
797 30°C with shaking. Cultures were centrifuged 5 min at 230 g and pellets were washed with
798 sterile PBS. Cultures were centrifuged again and pellets were resuspended in 200 µL sterile
799 PBS with 0.2% glucose. Cultures were incubated an extra 30 min at 30°C to activate energy-
800 dependent efflux, then diluted 1:10 prior to fluorescence measurements by flow cytometry.
801 Fluorescence in the green and orange channels using blue and green lasers, respectively,
802 was acquired for approximately 2,000 events per sample with a guava easyCyte HT
803 cytometer (Cytek). Fluorescence values in both channels were normalized with the cell size
804 using the FSC value. Thresholds were set for both normalized fluorescence values to
805 maximize events with fluorescence below the thresholds for the negative control (sample not

806 treated with rhodamine), as well as maximize events with fluorescence above the thresholds
807 for the positive control (s_012 in Supp Data 1). The percentage of cells with fluorescence
808 above both thresholds is considered to be inversely correlated with the efflux capacity.

809 Fluorescence reporter assay

810 A GFP reporter was used to evaluate the level of expression of *FCY1* in one of the parental
811 strains to assess *FCY1* functionality. Precultures of LL13-040 with or without *FCY1-mEGFP*
812 (s_002 and s_003 in Supp Data 1) were prepared from single colonies in 5 mL YPD medium
813 and incubated overnight at 30°C with shaking. Precultures were diluted at 1.5 OD_{600} in sterile
814 water. 24-well plates containing either SC, SC -ura, SD (MSG) or SD (NH_4) with 0, 0.78 or
815 1.56 µg/mL 5-FC were inoculated at 0.15 OD_{600}, sealed with porous adhesive film and
816 incubated for 4 h at 30°C with shaking. Cultures were diluted at 0.05 OD_{600}. Fluorescence in
817 the green channel using a blue laser was acquired for 5,000 events. Events with a SSC
818 value (proxy for cell granularity) below 300 or a FSC value (proxy for cell size) below 2,000
819 were filtered out. The fluorescence values were normalized by the FSC value.

820 DNA extraction and sequencing

821 In order to identify which mutation(s) were conferring 5-FC resistance in *rho*$^+$ mutants, we
822 performed whole-genome sequencing. The mutants were cultured overnight at 30°C in 24-
823 well plates with 2 mL YPD, sealed with porous adhesive film. Cells were pelleted from a total
824 of approximately 20 OD units per sample. DNA was extracted using the MasterPure Yeast
825 DNA Purification kit (Epicentre) following the kit's protocol, except for the following
826 adjustments. Isopropanol precipitation was performed for 1 h at room temperature. Pellets
827 were dried at 55°C for 25 min, after which they were resuspended in 50 µL 0.2 ng/µL RNase.
828 Samples were incubated an additional 5 min at 55°C, then immediately purified using SPRI
829 beads (1:1 ratio, Axygen). Attempts to extract genomic DNA from *rho*$^-$ mutants proved
830 unsuccessful with this method.

Genomic DNA was stored at -20°C, then quantified in technical triplicates using the AccuClear Ultra High Sensitivity dsDNA Quantitation kit. A total of 282 samples (276 out of 294 rearrayed *rho*$^+$ mutants, as well as the parental strain and the *fcy1*Δ and *fcy2*Δ mutants for each background, s_004/5/9/10) were diluted to 10 ng/µL for a total of 40 ng and arranged on three 96-well plates. For eight samples, whose initial concentration was too low, a volume of 15 µL was pipetted and dried in a SpeedVac, then resuspended in the appropriate volume to the desired final concentration of 10 ng/uL. Sequencing libraries were prepared using the Riptide High Throughput Rapid DNA Library Prep kit (iGenomx), according to the kit's protocol. The three 96-well plates were each pooled separately. For the amplification step, we modified the protocol to use barcoded primers for each pool instead of a single universal PCR primer. The three pools were SPRI-purified in two steps with protocol option 3 (recommended for PE150 sequencing). The pools were checked on agarose gel, quantified with the AccuClear Ultra High Sensitivity dsDNA Quantitation kit and analyzed on BioAnalyzer (Agilent). Finally, they were sequenced in paired-end 150 bp on an Illumina NovaSeq 6000 S4 system at the Centre d'expertise et de services Génome Québec.

FCY1 and *FUR1* were amplified from the same genomic DNA using primers listed in Supp Data 1, then sequenced by Sanger amplicon sequencing. For *FUR1* amplicons, all samples for which enough material could be recovered (after preparing WGS libraries) were processed. The reactions were performed at the Centre Hospitalier de l'Université Laval sequencing platform (Université Laval, Québec).

Validations and complementations

Once we identified *FUR1* as being the hotspot for mutations in *rho*$^+$ mutants, we confirmed the detected mutations were causal by using two types of growth assays: *validation* refers to a growth assay in isolated liquid medium where we compared the growth of mutants to that

of the *fur1*Δ mutant, whereas *complementation* refers to measuring the growth of mutants upon expression of the WT allele of *FUR1* carried by a plasmid.

Validations

35 *rho*$^+$ mutants (LL13-040; n=17, NC-02, n=18), the deletion mutants for *FCY1*, *FCY2* and *FUR1* (s_004/5/6/9/10/11 in Supp Data 1) and both parental strains were precultured in duplicates in a single 96-deep-well plate with 1 mL YPD overnight at 30°C with shaking. Precultures were diluted at 1 OD_{600} in sterile water and inoculated at a final concentration of 0.1 OD_{600} in two sterile Greiner 96-well plates with SD or SD + 100 µg/mL 5-FC. OD_{600} measurements were performed at 30°C every 15 min until a plateau was reached in a Tecan Infinite M Nano (Tecan Life Sciences).

Complementations

32 out of the 35 validation mutants (16 from each background) and the *fur1*Δ mutants were transformed with pMoBY or pMoBY-*FUR1* [72] using a modified yeast transformation method [73]. Transformants were selected with combinations of nourseothricin or hygromycin B and G418. Precultures were prepared in a single 96-deep-well plate with 1 mL YPD + G418, inoculated from a single colony for each strain and incubated overnight at 30°C with shaking. Precultures were diluted at 1 OD_{600} in sterile water and inoculated at a final concentration of 0.1 OD_{600} in a sterile Greiner 96-well plate with SD + 100 µg/mL 5-FC. OD_{600} measurements were performed at 30°C every 15 min until a plateau was reached in a BioTek Epoch 2 Microplate Spectrophotometer (Agilent).

Growth assays in isolated liquid cultures

Three types of growth assays in isolated liquid cultures were carried out. 1- ‘Small-scale’ assays (precultures in 5 mL tubes and growth measurements in 96-well plates) were used a) to evaluate 5-FC sensitivity in different media (minimal and rich) and b) to measure the

growth of parental strains in minimal medium with different sources of nitrogen. 2- A single 'larger-scale' growth assay (precultures in 96-well plates and growth measurements in 384-well plate) was used to measure the growth of a subset of *rho*$^{+}$ mutants, as well as the *fcy1*Δ mutant, in liquid medium, in order to compare with the growth measured on solid medium. 3- A dose-response curve assay was used to measure the inhibition coefficient corresponding to the 5-FC concentration used in the evolution experiment.

'Small-scale' growth assay

For the 'small-scale' growth assays, strains were streaked on YPD agar medium supplemented with the appropriate antibiotics. Precultures were prepared from three isolated colonies in 5 mL YPD medium with appropriate selection and incubated overnight at 30°C with shaking. Precultures were diluted at 1 OD_{600} in sterile water. Sterile Greiner 96-well plates were prepared with the indicated culture medium and compounds and cultures were inoculated at a final concentration of 0.1 OD_{600}. OD_{600} measurements were performed at 30°C every 15 min until a plateau was reached in a Tecan Infinite M Nano (Tecan Life Sciences).

'Larger-scale' growth assay

For the 'larger-scale' growth assay, precultures were prepared in a 96-deep-well plate with 1 mL YPD and incubated overnight at 30°C with shaking. Precultures were diluted at 1 OD_{600} in sterile water. A sterile 384-well plate containing four different conditions was used: SD, SD + 25 µg/mL 5-FC, SD + 100 µg/mL 5-FC and YNB + 2% glucose + 250 µg/mL cytosine. The lid was conditioned by incubating 3 min with 5 mL 0.05% Triton X-100 / 20% ethanol and dried under sterile conditions. Cultures were inoculated in a single replicate at a final concentration of 0.1 OD_{600} in a final volume of 80 µL per well. OD_{600} measurements were

905 performed at 30°C every 15 min in a Tecan Spark (Tecan Life Sciences) with an active
906 Tecool temperature control module, until curves showed signs of evaporation (13 h).

907 Dose-response curve assay

908 A single 96-well plate was prepared as described for the 'small-scale' growth assays, with
909 cultures of LL13-040 and NC-02 in biological triplicates. 5-FC was serially diluted 1:2 seven
910 times starting from a final concentration of 3.125 µg/mL. The maximum growth rate was
911 transformed into the inhibition coefficient, with an inhibition coefficient of 0 corresponding to
912 the maximum growth rate measured in the absence of 5-FC.

913 Assessment of cross-feeding-induced toxicity

914 Three types of growth-based assays were carried out to investigate the selection of *fur1*$^-$
915 mutants over *fcy1*$^-$ mutants. A liquid medium conditioning assay was used to evaluate if a
916 toxic compound was secreted by the *fur1*Δ mutant. A competition assay was used to assess
917 the importance of cell density in liquid medium. Finally, an inhibition assay was performed to
918 confirm the phenotype on solid medium.

919 Medium conditioning assay

920 Precultures of LL13-040 and NC-02 with or without deletion of *FCY1* or *FUR1*
921 (s_002/4/6/8/9/11) were prepared from three isolated colonies in 5 mL YPD medium and
922 incubated overnight at 30°C with shaking. Precultures were diluted at 1 OD_{600} in sterile
923 water. Subcultures of 5 mL SD medium with or without 1.56 µg/mL 5-FC in 50 mL Falcon
924 tubes were inoculated at a final concentration of 0.1 OD_{600}. After a 5h incubation at 30°C
925 with shaking, cultures had reached 0.5-0.6 OD_{600}. Cultures were centrifuged 5 min at 500 g
926 and the supernatants were filtered, then transferred to a sterile Greiner 96-well plate. The
927 media "conditioned" by the growth of the *fcy1*Δ mutant were inoculated with either the *FUR1*
928 null mutant or the WT. The media conditioned by the growth of the *FUR1* null mutant were

929 inoculated with either the *fcy1*Δ mutant or the WT. Cultures were inoculated at a final
930 concentration of 0.1 OD_{600}. Growth curves were acquired as described above.

931 Competition assay

932 Precultures of LL13-040 and NC-02 with or without deletion of *FCY1* or *FUR1*
933 (s_002/4/6/8/9/11) were prepared as described above. Precultures were diluted at 1 OD_{600} in
934 sterile water. Subcultures of 5 mL SD medium without 5-FC were inoculated at a final
935 concentration of 0.1 OD_{600}. After a 5h incubation at 30°C with shaking, cultures had reached
936 0.6 OD_{600}. For each background, cultures of both deletion mutants were pooled in equal
937 volumes and serially diluted in sterile water. 0.5 mL of each dilution (10^{-3}, 10^{-4} and 10^{-5} OD)
938 was plated on large petri dishes containing SD with 1.56 µg/mL 5-FC. From each plate, 16
939 colonies were streaked on the same medium to make sure they were 5-FC resistant.
940 Additionally, the genotype (*fcy1*Δ or *fur1*Δ) was identified by multiplexed colony-PCR using
941 one common primer annealing in either marker (*NAT* or *HPH*) and two gene-specific primers
942 annealing upstream the deletion site. The reported CFU counts correspond to the mean of 2
943 replicate experiments, but the statistical test (Chi-square of independence) was performed
944 on the cumulative sum of counts.

945 Inhibition assay

946 Precultures of LL13-040 and NC-02 with or without deletion of *FCY1* or *FUR1*
947 (s_002/4/6/8/9/11) were prepared from three isolated colonies in 5 mL YPD medium and
948 incubated overnight at 30°C with shaking.

Computational analyses

WGS data

FASTQ reads were demultiplexed (and adapter-trimmed) using DemuxFastqs from the fgbio set of tools. A custom snakemake pipeline was used to process the FASTQ files [74]. Reads were aligned using bwa-mem2 on the reference S288C genome [75]. Aligned reads were sorted and indexed using samtools [76]. Reads that did not map uniquely (SAM FLAG 256) were excluded. PCR duplicates were removed using picard's MarkDuplicates. Reads around indels were realigned using samtools calmd. The pipeline was run on the IBIS servers.

Variant calling

Variants were called with two methods, bcftools/samtools and GATK.

SNP calling with samtools/bcftools ("samtools")

SNP calling was conducted with bcftools v1.9. SNP pileup was generated with bcftools mpileup command with options -C50, -min-MQ 4, -min-BQ 13 and prior removal of reads that were unmapped, not in primary alignment, failing quality checks or were PCR/optical duplicates. The command was run separately for samples from the two backgrounds (LL13-040 and NC-02). Haploid SNP calling was conducted with bcftools call command with option -mv.

SNP calling with gatk ("gatk")

In the second variant calling method, bam files were edited using picard v2.18 (http://broadinstitute.github.io/picard/), SNP and indel calling was conducted with GATK v4.2.6.1 [77]. Prior to variant calling, an RG (read group) tag was added to individual bam files. GVCF files were generated with GATK HaplotypeCaller, with options -ploidy 1 -ERC GVCF and --min-base-quality-score 20. GVCF files of samples coming from the same

973 background (LL13-040 or NC-02) were combined with GATK CombineGVCFs, genotyped
974 with GATK GenotypeGVCFs, and processed separately. SNPs with the following criteria
975 were filtered out: variant quality score (QUAL) < 30, QUAL by depth (QD) < 2, mapping
976 quality (MQ) < 40, Fisher's exact tests of strand bias (FS) > 60, symmetric odds ratio test of
977 strand bias (SOR) > 4, mapping quality rank sum test (MQRankSum) < -12.5, and rank sum
978 test for site position within reads (ReadPosRankSum) < -8. Indels were filtered out if they
979 met the following criteria: QD < 2, QUAL < 30, FS > 200, or ReadPosRankSum < -20.
980
981 Further filtering was conducted for all variant sets with bcftools v1.9 and python v3.10
982 scripts. We applied a set of filtering criteria both to samples, and variants. First, we removed
983 samples (marked as missing data), which met the following criteria: read depth < 4, allelic
984 depth (AD) for the second most common allele > 4, ratio of the AD of the second to the first
985 most common allele > 0.2. Then, variants meeting the following criteria were removed: mean
986 read depth across all samples < 10, total read depth > 20000, variant quality (QUAL) < 20,
987 mapping quality (MQ) < 40, high frequency (allele frequency (AF) > 0.99 or allele count (AC)
988 = 0). Finally, any variants shared with the parental strain were removed as well. Variants
989 were ultimately annotated with SnpEff v5.0 [78] using *S. cerevisiae* genome vR64-3-1.

990 ## CNVs

991 Coverage of WGS data was analyzed to look for regions with copy number variations (larger
992 than 5,000 bp and smaller than half of the chromosome length). Read count per position for
993 each sample was output using samtools depth. Mean read count was calculated in non-
994 overlapping windows of 5,000 bp and corrected for mapping bias related to GC content.
995 Namely, the read count in each window ("W") was multiplied by a ratio of median read count
996 over all windows divided by a median read count over all windows with the same GC as "W".
997 End chromosome bias (increasing read count towards chromosome ends) was corrected by
998 fitting a curve for the windows closest to one chromosome end (each half of the
999 chromosome), using the LOWESS smoothing method, in python v3 statsmodels package,

with a default of 2/3 of data points to estimate each y value. Windows were then divided by the fitted line to obtain the normalized read count.

Predictions of impact of mutations

Mutations were submitted to the online tool mutfunc to predict their impact, notably on stability and/or conservation in a homology model [79].

Data availability

All sequencing data are available at the NCBI Sequence Read Archive (SRA) under BioProject PRJNA952138. Details on demultiplexing are provided in Supp Data 4. All scripts (analyses and figure generation) are available on the dedicated repository. Strains are available upon request.

Acknowledgments

We thank Justin C. Fay for the kind gift of NC-02, Philippe Després for important insights on pyrimidine cross-feeding, Mathieu Hénault for technical assistance, Isabelle Gagnon-Arsenault for critical reading of the manuscript and members of the Landry lab for feedback on the project.

Funding

This work was supported by the Canadian Institutes of Health Research (CIHR) (Foundation grant 387697 to CRL) and a Genome Canada and Genome Quebec grant (grant 6569 to CRL). CRL holds a Canada Research Chair in Cellular Systems and Synthetic Biology. RD is supported by a Fonds de Recherche du Québec - Santé (FRQS) postdoctoral fellowship.

AF was supported by LSARP Genome Canada (grant 10106), and an NSERC Discovery grant (RGPIN-2020-04844 to CRL).

Conflicts of interest

None declared.

References

1. QuickStats: Death Rate* From Complications of Medical and Surgical Care Among Adults Aged ≥45 Years, by Age Group — United States, 1999–2009. 21 Sep 2012 [cited 10 Mar 2023]. Available: https://www.cdc.gov/mmwr/preview/mmwrhtml/mm6137a6.htm

2. The top 10 causes of death. [cited 10 Mar 2023]. Available: https://www.who.int/news-room/fact-sheets/detail/the-top-10-causes-of-death

3. Robbins N, Caplan T, Cowen LE. Molecular Evolution of Antifungal Drug Resistance. Annu Rev Microbiol. 2017;71: 753–775.

4. Armstrong-James D, Meintjes G, Brown GD. A neglected epidemic: fungal infections in HIV/AIDS. Trends Microbiol. 2014;22: 120–127.

5. Alcazar-Fuoli L, Mellado E. Current status of antifungal resistance and its impact on clinical practice. Br J Haematol. 2014;166: 471–484.

6. CDC. Antibiotic Resistance Threats in the United States, 2019. Atlanta, GA: US Department of Health and Human Services, CDC. 2019; 148.

7. Vanreppelen G, Wuyts J, Van Dijck P, Vandecruys P. Sources of Antifungal Drugs. J Fungi (Basel). 2023;9. doi:10.3390/jof9020171

8. Desai JV, Mitchell AP, Andes DR. Fungal biofilms, drug resistance, and recurrent

infection. Cold Spring Harb Perspect Med. 2014;4. doi:10.1101/cshperspect.a019729

9. Perlin DS, Wiederhold NP. Culture-Independent Molecular Methods for Detection of Antifungal Resistance Mechanisms and Fungal Identification. J Infect Dis. 2017;216: S458–S465.

10. Web, Annex A. World Health Organization Model List of Essential Medicines – 23rd List, 2023. 2023.

11. Delma FZ, Al-Hatmi AMS, Brüggemann RJM, Melchers WJG, de Hoog S, Verweij PE, et al. Molecular Mechanisms of 5-Fluorocytosine Resistance in Yeasts and Filamentous Fungi. J Fungi (Basel). 2021;7. doi:10.3390/jof7110909

12. Bennet JE. Flucytosine. Ann Intern Med. 1977;86: 319–321.

13. Paluszynski JP, Klassen R, Rohe M, Meinhardt F. Various cytosine/adenine permease homologues are involved in the toxicity of 5-fluorocytosine in Saccharomyces cerevisiae. Yeast. 2006;23: 707–715.

14. Longley DB, Harkin DP, Johnston PG. 5-fluorouracil: mechanisms of action and clinical strategies. Nat Rev Cancer. 2003;3: 330–338.

15. Santi DV, McHenry CS, Sommer H. Mechanism of interaction of thymidylate synthetase with 5-fluorodeoxyuridylate. Biochemistry. 1974;13: 471–481.

16. Kufe DW, Major PP. 5-Fluorouracil incorporation into human breast carcinoma RNA correlates with cytotoxicity. J Biol Chem. 1981;256: 9802–9805.

17. Hope WW, Tabernero L, Denning DW, Anderson MJ. Molecular mechanisms of primary resistance to flucytosine in Candida albicans. Antimicrob Agents Chemother. 2004;48: 4377–4386.

18. McManus BA, Moran GP, Higgins JA, Sullivan DJ, Coleman DC. A Ser29Leu

substitution in the cytosine deaminase Fca1p is responsible for clade-specific flucytosine resistance in Candida dubliniensis. Antimicrob Agents Chemother. 2009;53: 4678–4685.

19. Edlind TD, Katiyar SK. Mutational Analysis of Flucytosine Resistance in Candida glabrata. Antimicrob Agents Chemother. 2010;54: 4733–4738.

20. Florent M, Noël T, Ruprich-Robert G, Da Silva B, Fitton-Ouhabi V, Chastin C, et al. Nonsense and missense mutations in FCY2 and FCY1 genes are responsible for flucytosine resistance and flucytosine-fluconazole cross-resistance in clinical isolates of Candida lusitaniae. Antimicrob Agents Chemother. 2009;53: 2982–2990.

21. Costa C, Henriques A, Pires C, Nunes J, Ohno M, Chibana H, et al. The dual role of candida glabrata drug:H+ antiporter CgAqr1 (ORF CAGL0J09944g) in antifungal drug and acetic acid resistance. Front Microbiol. 2013;4: 170.

22. Steier Z, Vermitsky J-P, Toner G, Gygax SE, Edlind T, Katiyar S. Flucytosine antagonism of azole activity versus Candida glabrata: role of transcription factor Pdr1 and multidrug transporter Cdr1. Antimicrob Agents Chemother. 2013;57: 5543–5547.

23. Costa C, Ponte A, Pais P, Santos R, Cavalheiro M, Yaguchi T, et al. New Mechanisms of Flucytosine Resistance in C. glabrata Unveiled by a Chemogenomics Analysis in S. cerevisiae. PLoS One. 2015;10: e0135110.

24. Pais P, Pires C, Costa C, Okamoto M, Chibana H, Teixeira MC. Membrane Proteomics Analysis of the Candida glabrata Response to 5-Flucytosine: Unveiling the Role and Regulation of the Drug Efflux Transporters CgFlr1 and CgFlr2. Front Microbiol. 2016;7: 2045.

25. Kannan A, Asner SA, Trachsel E, Kelly S, Parker J, Sanglard D. Comparative Genomics for the Elucidation of Multidrug Resistance in Candida lusitaniae. MBio. 2019;10. doi:10.1128/mBio.02512-19

1089 26. Paul S, Moye-Rowley WS. Multidrug resistance in fungi: regulation of transporter-
1090 encoding gene expression. Front Physiol. 2014;5: 143.

1091 27. Séron K, Blondel MO, Haguenauer-Tsapis R, Volland C. Uracil-induced down-regulation
1092 of the yeast uracil permease. J Bacteriol. 1999;181: 1793–1800.

1093 28. Gerstein AC, Berman J. Candida albicans Genetic Background Influences Mean and
1094 Heterogeneity of Drug Responses and Genome Stability during Evolution in
1095 Fluconazole. mSphere. 2020;5. doi:10.1128/mSphere.00480-20

1096 29. Ljungdahl PO, Daignan-Fornier B. Regulation of Amino Acid, Nucleotide, and
1097 Phosphate Metabolism in Saccharomyces cerevisiae. Genetics. 2012-3;190: 885–929.

1098 30. Lacroute F. Regulation of pyrimidine biosynthesis in Saccharomyces cerevisiae. J
1099 Bacteriol. 1968;95: 824–832.

1100 31. Liljelund P, Lacroute F. Genetic characterization and isolation of theSaccharomyces
1101 cerevisiae gene coding for uridine monophosphokinase. Mol Gen Genet. 1986;205: 74–
1102 81.

1103 32. Kurtz JE, Exinger F, Erbs P, Jund R. New insights into the pyrimidine salvage pathway
1104 of Saccharomyces cerevisiae: requirement of six genes for cytidine metabolism. Curr
1105 Genet. 1999;36: 130–136.

1106 33. Erbs P, Exinger F, Jund R. Characterization of the Saccharomyces cerevisiae FCY1
1107 gene encoding cytosine deaminase and its homologue FCA1 of Candida albicans. Curr
1108 Genet. 1997;31: 1–6.

1109 34. Kern L, de Montigny J, Jund R, Lacroute F. The FUR1 gene of Saccharomyces
1110 cerevisiae: cloning, structure and expression of wild-type and mutant alleles. Gene.
1111 1990;88: 149–157.

1112 35. Polak A, Scholer HJ. Mode of action of 5-fluorocytosine and mechanisms of resistance.

Chemotherapy. 1975;21: 113–130.

36. Fasoli MO, Kerridge D, Morris PG, Torosantucci A. 19F nuclear magnetic resonance study of fluoropyrimidine metabolism in strains of Candida glabrata with specific defects in pyrimidine metabolism. Antimicrob Agents Chemother. 1990;34: 1996–2006.

37. Jumper J, Evans R, Pritzel A, Green T, Figurnov M, Ronneberger O, et al. Highly accurate protein structure prediction with AlphaFold. Nature. 2021;596: 583–589.

38. Varadi M, Anyango S, Deshpande M, Nair S, Natassia C, Yordanova G, et al. AlphaFold Protein Structure Database: massively expanding the structural coverage of protein-sequence space with high-accuracy models. Nucleic Acids Res. 2022;50: D439–D444.

39. Maesaki S, Marichal P, Vanden Bossche H, Sanglard D, Kohno S. Rhodamine 6G efflux for the detection of CDR1-overexpressing azole-resistant Candida albicans strains. J Antimicrob Chemother. 1999;44: 27–31.

40. Pettersen EF, Goddard TD, Huang CC, Meng EC, Couch GS, Croll TI, et al. UCSF ChimeraX: Structure visualization for researchers, educators, and developers. Protein Sci. 2021;30: 70–82.

41. Després PC, Cisneros AF, Alexander EMM, Sonigara R, Gagné-Thivierge C, Dubé AK, et al. Asymmetrical dose responses shape the evolutionary trade-off between antifungal resistance and nutrient use. Nat Ecol Evol. 2022;6: 1501–1515.

42. Hallstrom TC, Moye-Rowley WS. Multiple signals from dysfunctional mitochondria activate the pleiotropic drug resistance pathway in Saccharomyces cerevisiae. J Biol Chem. 2000;275: 37347–37356.

43. Ferrari S, Sanguinetti M, De Bernardis F, Torelli R, Posteraro B, Vandeputte P, et al. Loss of Mitochondrial Functions Associated with Azole Resistance in Candida glabrata Results in Enhanced Virulence in Mice. Antimicrob Agents Chemother. 2011;55: 1852–

1860.

44. Taylor MB, Skophammer R, Warwick AR, Geck RC, Boyer JM, yEvo Students, et al. yEvo: experimental evolution in high school classrooms selects for novel mutations that impact clotrimazole resistance in Saccharomyces cerevisiae. G3 . 2022;12. doi:10.1093/g3journal/jkac246

45. K Redhu A, Shah AH, Prasad R. MFS transporters of Candida species and their role in clinical drug resistance. FEMS Yeast Res. 2016;16. doi:10.1093/femsyr/fow043

46. Cuenca-Estrella M, Díaz-Guerra TM, Mellado E, Rodríguez-Tudela JL. Flucytosine primary resistance in Candida species and Cryptococcus neoformans. Eur J Clin Microbiol Infect Dis. 2001;20: 276–279.

47. Bouchara J-P, Zouhair R, LE Boudouil S, Renier G, Filmon R, Chabasse D, et al. In-vivo selection of an azole-resistant petite mutant of Candida glabrata. J Med Microbiol. 2000;49: 977–984.

48. Chapeland-Leclerc F, Hennequin C, Papon N, Noël T, Girard A, Socié G, et al. Acquisition of flucytosine, azole, and caspofungin resistance in Candida glabrata bloodstream isolates serially obtained from a hematopoietic stem cell transplant recipient. Antimicrob Agents Chemother. 2010;54: 1360–1362.

49. Rhodes J, Abdolrasouli A, Farrer RA, Cuomo CA, Aanensen DM, Armstrong-James D, et al. Genomic epidemiology of the UK outbreak of the emerging human fungal pathogen Candida auris. Emerg Microbes Infect. 2018;7: 43.

50. Chang YC, Lamichhane AK, Cai H, Walter PJ, Bennett JE, Kwon-Chung KJ. Moderate levels of 5-fluorocytosine cause the emergence of high frequency resistance in cryptococci. Nat Commun. 2021;12: 3418.

51. Charlier C, El Sissy C, Bachelier-Bassi S, Scemla A, Quesne G, Sitterlé E, et al.

Acquired Flucytosine Resistance during Combination Therapy with Caspofungin and Flucytosine for Candida glabrata Cystitis. Antimicrob Agents Chemother. 2016;60: 662–665.

52. Ono J, Gerstein AC, Otto SP. Widespread Genetic Incompatibilities between First-Step Mutations during Parallel Adaptation of Saccharomyces cerevisiae to a Common Environment. PLoS Biol. 2017;15: e1002591.

53. Shahi G, Kumar M, Skwarecki AS, Edmondson M, Banerjee A, Usher J, et al. Fluconazole resistant Candida auris clinical isolates have increased levels of cell wall chitin and increased susceptibility to a glucosamine-6-phosphate synthase inhibitor. Cell Surf. 2022;8: 100076.

54. Lara-Aguilar V, Rueda C, García-Barbazán I, Varona S, Monzón S, Jiménez P, et al. Adaptation of the emerging pathogenic yeast Candida auris to high caspofungin concentrations correlates with cell wall changes. Virulence. 2021;12: 1400–1417.

55. Walker LA, Munro CA, de Bruijn I, Lenardon MD, McKinnon A, Gow NAR. Stimulation of chitin synthesis rescues Candida albicans from echinocandins. PLoS Pathog. 2008;4: e1000040.

56. Giaever G, Chu AM, Ni L, Connelly C, Riles L, Véronneau S, et al. Functional profiling of the Saccharomyces cerevisiae genome. Nature. 2002;418: 387–391.

57. Carlsson M, Gustavsson M, Hu G-Z, Murén E, Ronne H. A Ham1p-Dependent Mechanism and Modulation of the Pyrimidine Biosynthetic Pathway Can Both Confer Resistance to 5-Fluorouracil in Yeast. PLoS One. 2013;8. doi:10.1371/journal.pone.0052094

58. Whelan WL. The genetic basis of resistance to 5-fluorocytosine in Candida species and Cryptococcus neoformans. Crit Rev Microbiol. 1987;15: 45–56.

1185 59. Papon N, Noël T, Florent M, Gibot-Leclerc S, Jean D, Chastin C, et al. Molecular
1186 Mechanism of Flucytosine Resistance in Candida lusitaniae: Contribution of the FCY2,
1187 FCY1, and FUR1 Genes to 5-Fluorouracil and Fluconazole Cross-Resistance.
1188 Antimicrob Agents Chemother. 2007;51: 369–371.

1189 60. Das SG, Direito SO, Waclaw B, Allen RJ, Krug J. Predictable properties of fitness
1190 landscapes induced by adaptational tradeoffs. Elife. 2020;9. doi:10.7554/eLife.55155

1191 61. Moreno-Gamez S, Hill AL, Rosenbloom DIS, Petrov DA, Nowak MA, Pennings PS.
1192 Imperfect drug penetration leads to spatial monotherapy and rapid evolution of multidrug
1193 resistance. Proc Natl Acad Sci U S A. 2015;112: E2874–83.

1194 62. Alexander HK, MacLean RC. Stochastic bacterial population dynamics restrict the
1195 establishment of antibiotic resistance from single cells. Proc Natl Acad Sci U S A.
1196 2020;117: 19455–19464.

1197 63. Todd RT, Soisangwan N, Peters S, Kemp B, Crooks T, Gerstein A, et al. Antifungal
1198 Drug Concentration Impacts the Spectrum of Adaptive Mutations in Candida albicans.
1199 Mol Biol Evol. 2023;40. doi:10.1093/molbev/msad009

1200 64. Ramage G, Martínez JP, López-Ribot JL. Candida biofilms on implanted biomaterials: a
1201 clinically significant problem. FEMS Yeast Res. 2006;6: 979–986.

1202 65. Leducq J-B, Nielly-Thibault L, Charron G, Eberlein C, Verta J-P, Samani P, et al.
1203 Speciation driven by hybridization and chromosomal plasticity in a wild yeast. Nat
1204 Microbiol. 2016;1: 15003.

1205 66. Bleykasten-Grosshans C, Friedrich A, Schacherer J. Genome-wide analysis of
1206 intraspecific transposon diversity in yeast. BMC Genomics. 2013;14: 399.

1207 67. Gerstein AC, Lo DS, Otto SP. Parallel Genetic Changes and Nonparallel Gene–
1208 Environment Interactions Characterize the Evolution of Drug Resistance in Yeast.

Genetics. 09/2012;192: 241–252.

68. van der Walt S, Schönberger JL, Nunez-Iglesias J, Boulogne F, Warner JD, Yager N, et al. scikit-image: image processing in Python. PeerJ. 2014;2: e453.

69. Kamrad S, Rodríguez-López M, Cotobal C, Correia-Melo C, Ralser M, Bähler J. Pyphe, a python toolbox for assessing microbial growth and cell viability in high-throughput colony screens. Elife. 2020;9. doi:10.7554/eLife.55160

70. Revie NM, Robbins N, Whitesell L, Frost JR, Appavoo SD, Yudin AK, et al. Oxadiazole-Containing Macrocyclic Peptides Potentiate Azole Activity against Pathogenic Candida Species. mSphere. 2020;5. doi:10.1128/mSphere.00256-20

71. Celaj A, Gebbia M, Musa L, Cote AG, Snider J, Wong V, et al. Highly Combinatorial Genetic Interaction Analysis Reveals a Multi-Drug Transporter Influence Network. Cell Syst. 2020;10: 25–38.e10.

72. Ho CH, Magtanong L, Barker SL, Gresham D, Nishimura S, Natarajan P, et al. A molecular barcoded yeast ORF library enables mode-of-action analysis of bioactive compounds. Nat Biotechnol. 2009;27: 369–377.

73. Kaiser C, Michaelis S, Mitchell A. Modified Lithium Acetate Yeast Transformation. Methods in Yeast Genetics, Cold Spring Harbor Laboratory Course Manual, 1994 Edition. Cold Spring Harbor Laboratory Press; 1994. p. 201.

74. Mölder F, Jablonski KP, Letcher B, Hall MB, Tomkins-Tinch CH, Sochat V, et al. Sustainable data analysis with Snakemake. F1000Res. 2021;10: 33.

75. Vasimuddin M, Misra S, Li H, Aluru S. Efficient Architecture-Aware Acceleration of BWA-MEM for Multicore Systems. 2019 IEEE International Parallel and Distributed Processing Symposium (IPDPS). 2019. pp. 314–324.

76. Danecek P, Bonfield JK, Liddle J, Marshall J, Ohan V, Pollard MO, et al. Twelve years

of SAMtools and BCFtools. Gigascience. 2021;10. doi:10.1093/gigascience/giab008

77. Poplin R, Ruano-Rubio V, DePristo MA, Fennell TJ, Carneiro MO, Van der Auwera GA, et al. Scaling accurate genetic variant discovery to tens of thousands of samples. bioRxiv. 2017. p. 201178. doi:10.1101/201178

78. Cingolani P, Platts A, Wang LL, Coon M, Nguyen T, Wang L, et al. A program for annotating and predicting the effects of single nucleotide polymorphisms, SnpEff: SNPs in the genome of Drosophila melanogaster strain w1118; iso-2; iso-3. Fly . 2012;6: 80–92.

79. Wagih O, Galardini M, Busby BP, Memon D, Typas A, Beltrao P. A resource of variant effect predictions of single nucleotide variants in model organisms. Mol Syst Biol. 2018;14: e8430.

Supporting information captions

Supp Fig 1. Growth of individual mutants on solid medium. Growth corresponds to the mean area under the curve (AUC, calculated on 22 h) from four replicate colonies, for individual strains arrayed on solid media: (A) YPD, SD, SD + 25 µg/mL 5-FC and SD + 6.25 µg/mL 5-FU, incubated at 30°C and (B) YPD, SD, SD + 25 µg/mL 5-FC, SD + 0.5 µg/mL micafungin, SD + 2 µg/mL caspofungin, SD + 16 µg/mL nystatin and SD + 64 µg/mL fluconazole, incubated at 37°C. Data correspond to Figs 2 and 3A before normalization with the WT, here represented as split violin plots. For both growth assays (corresponding to panels A and B), all *rho*$^{+}$ strains were gathered on a single plate, with WT controls for the two backgrounds (LL13-040 and NC-02). The mean AUC for the WT controls in each condition is indicated by a gray diamond. Similarly, the mean AUC for the WT controls present on plates with *rho*$^{-}$ strains (in this case, one plate for LL13-040 *rho*$^{-}$ strains and another for NC-02 *rho*$^{-}$ strains) is indicated by a red diamond.

Supp Fig 2. Depth per position. Normalized coverage calculated for 5 kb windows. Each track corresponds to a sequenced genome. Red signal indicates a normalized coverage above 4X. First page corresponds to LL13-040 genomes (B10, B11…) and second page to NC-02 genomes (B14, B15…).

Supp Fig 3. Diversity of Fur1 mutations per preculture. Each marker (dot or triangle) represents a single preculture, from which mutants were selected (# genomes). A gray dashed line indicates if as many mutations have been identified in Fur1 as the number of genomes that carried them. For one outlier (only three mutations found in 41 strains which arose from the same preculture), a pie chart details the corresponding mutations and the number of strains that carried them.

Supp Fig 4. Predicted impact of Fur1 mutations. Effect on stability (A) and conservation (B) of all possible amino acid substitutions in Fur1 which are predicted to be impactful by mutfunc [79]. Substitutions predicted to be non-deleterious are not shown. The substitutions captured in our dataset are highlighted (bigger colored dots). (A) Side plots indicate the kernel densities for all data points (lightgray) and substitutions captured in our dataset (black) along the position in Fur1 (top) or the ΔΔG value (right). (B) SIFT scores are represented on an inverted y-axis and are analogous to a *p*-value. Scores < 0.05 (gray dashed line) indicate a predicted deleterious mutation, with a low value (top of the plot) indicating that the amino acid change is very likely to affect protein function based on sequence conservation. For substitutions captured in our dataset, the color indicates the conservation level of the residue at that position.

Supp Fig 5. Location and type of detected mutations along the *FUR1* sequence. The location of all detected mutations in the *FUR1* gene sequence (n=118, length of the gene represented by a gray half-arrow) is indicated by a barplot (first track), where every bar

represents a unique mutation, and their height represents the number of unique genomes in which the mutation was identified. Bars are color-coded to indicate in which background the mutation was identified. The second and third tracks contain boolean indicators for the method of detection and the type of mutation (black for true, gray for false). On the third track, the corresponding positions along the Fur1 protein sequence are indicated.

Supp Fig 6. Fcy1 functionality in parental strains. A) Density plots showing the fluorescence signal of *FCY1*-mEGFP (green), compared to the control without fluorescent reporter (gray) in the background LL13-040. Signal was acquired by cytometry for 5,000 events. A single threshold (gray dashed line) was used to indicate relative percentages of events for both strains in each condition. B) Growth was measured for both parental strains in YNB + 2% glucose containing different nitrogen sources.

Supp Fig 7. Fcy1-mediated resistance in liquid and solid media. A) Growth assay in liquid medium. Cultures were inoculated from single replicates in a 384-well plate containing SD (control), SD + 25 µg/mL 5-FC (5-FC) or YNB + 2% glucose + 250 µg/mL cytosine (cytosine). Relative growth corresponds to the area under the curve (AUC, calculated on 13 h) normalized by the WT. B) Relative growth measured in liquid medium (data from panel A) compared to the one measured on solid medium for the corresponding mutants (data from Fig 2) at equal concentrations of 5-FC.

Supp Fig 8. 5-FU cross-feeding inhibition zones. Uncropped pictures as shown in Fig 6D.

Supp Fig 9. 5-FC dose response. A) Growth assays for LL13-040 in different media supplemented or not with either 1.56 or 3.125 µg/mL 5-FC: synthetic complete medium with standard drop-out mix (SC complete), SC without uracil (SC -ura), SD (MSG) with or without 0.2% aspartate and SD (NH_4) with or without 0.2% aspartate / 0.2% glutamate. The area under the curve (AUC) parameter was calculated from three biological replicates. B) 5-FC

dose-response curves in SD (MSG) for LL13-040 and NC-02. The concentration is shown on a log2 scale. 0 µg/mL 5-FC was used to normalize growth values. For each strain, the mean of three biological replicates for each concentration was used to fit the Hill equation. The corresponding IC50 and Hill coefficients are indicated.

Supp Fig 10. Growth measurements on YPG agar medium. A, B) Pictures of arrays on YPG agar medium after 22 h incubation at 30°C for LL13-040 (A) and NC-02 (B). Each mutant is spotted in four replicates with the *fcy1*Δ mutant occupying the border as positive control. Gray squares highlight mutants initially misannotated as *rho*$^-$. Pictures were cropped and converted into inverted gray levels for clarity and downstream analysis of colony size. C) Growth curves were obtained by automatic detection of colony size on transformed pictures taken every 2 h for 22 h at 30°C. Relative growth corresponds to the mean area under the curve (AUC) normalized by the WT. *rho*$^-$ mutants included in all other figures are colored in red. Gray dots correspond either to the WT control (on the dotted line corresponding to a relative fitness of 1), or to the misannotated mutants mentioned above, which were therefore excluded from all analyses except the rhodamine accumulation experiment.

Supp Data 1. Strains, plasmids and primers used in this study.

Supp Data 2. List of mutations detected in *FUR1*. Columns: SNP_pos_aa, 1-based position in the protein sequence of Fur1; mutation; mutID_true, unique mutation identifier (convertible to mutfunc-friendly format); mutation_type, SNP or indel; POS, position in chrVIII; pos_nt, 0-based position in the *FUR1* gene; REF, reference residue; ALT, alternative residue; detected_by, indicates if the mutation was detected by samtools, gatk or Sanger (1 row per detection method); RA_well, unique strain identifier and location on the plate after rearray; background; fluc_assay, iteration of the evolution experiment; pre_culture, indicates if the mutant was generated from the same preculture; Genomix_plate_nb, indicates on

1340 which plate the genomic DNA was located for WGS; val_comp, indicates if the mutant was
1341 tested in the validation assay and/or the complementation assay.
1342
1343 **Supp Data 3. Resistance-conferring mutations and their relative fitness at 30°C.**
1344 Columns: resistance gene; mutation; medium (YPD, SD, SD + 5-FC or SD + 5-FU); #
1345 strains, number of strains in which the mutation was detected across both backgrounds;
1346 median relative fitness.
1347
1348 **Supp Data 4. Illumina indexes and barcodes used for demultiplexing.** The master pool
1349 was demultiplexed using the i7 index at Genome Québec. The i5 index is provided but was
1350 not used for demultiplexing. Samples were demultiplexed from pools 1-3 using
1351 DemuxFastqs with read structure 8B12M+T 8M+T. Columns: pool; i7; i5; BioSample
1352 accession number; RA_well, unique strain identifier and location on the plate after rearray;
1353 sample barcode.

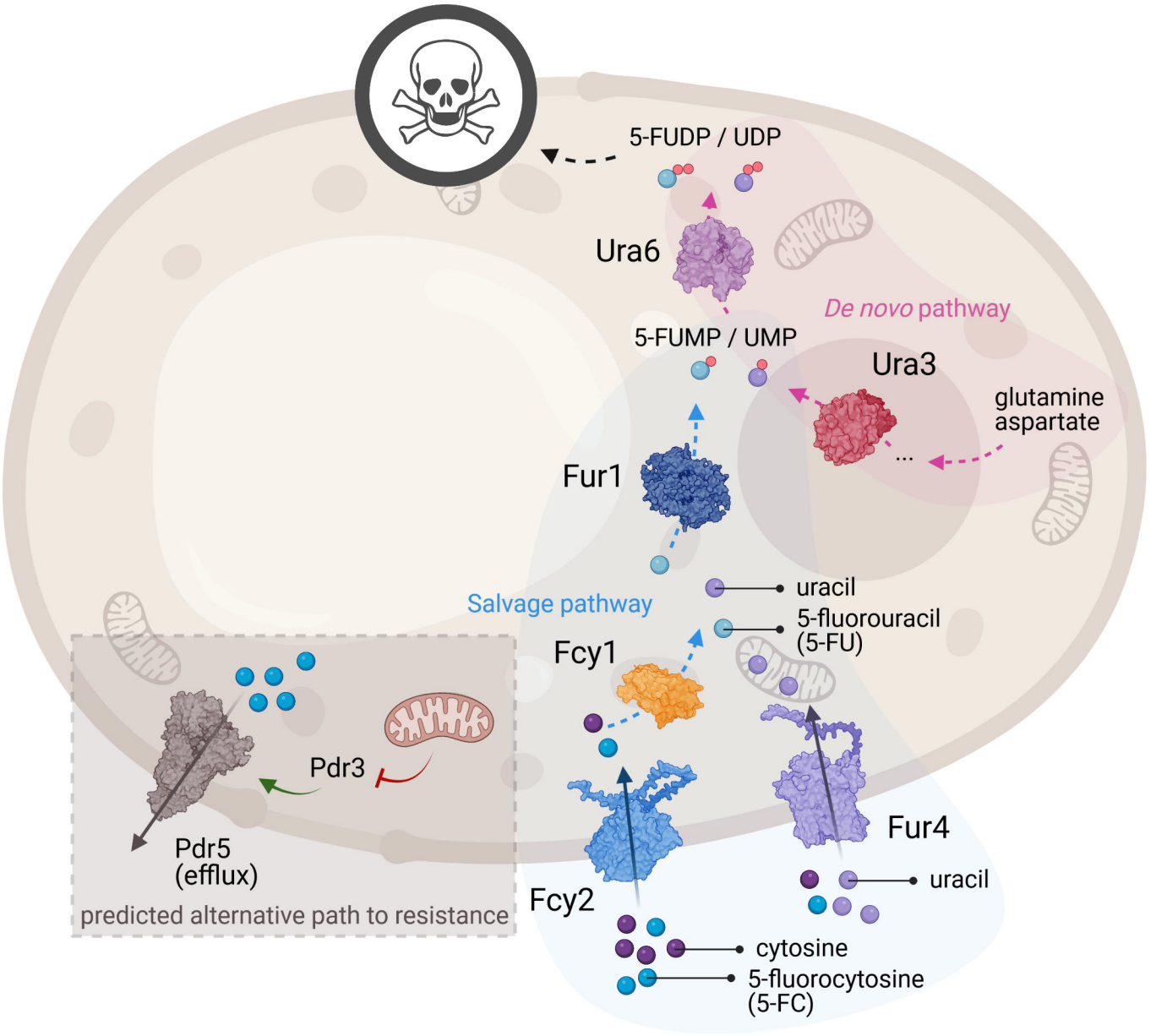
5-FUDP / UDP
Ura6
De novo pathway
5-FUMP / UMP
Ura3
glutamine
aspartate
...
Fur1
uracil
Salvage pathway
5-fluorouracil
(5-FU)
Fcy1
Pdr3
Pdr5
(efflux)
predicted alternative path to resistance
Fur4
uracil
Fcy2
cytosine
5-fluorocytosine
(5-FC)

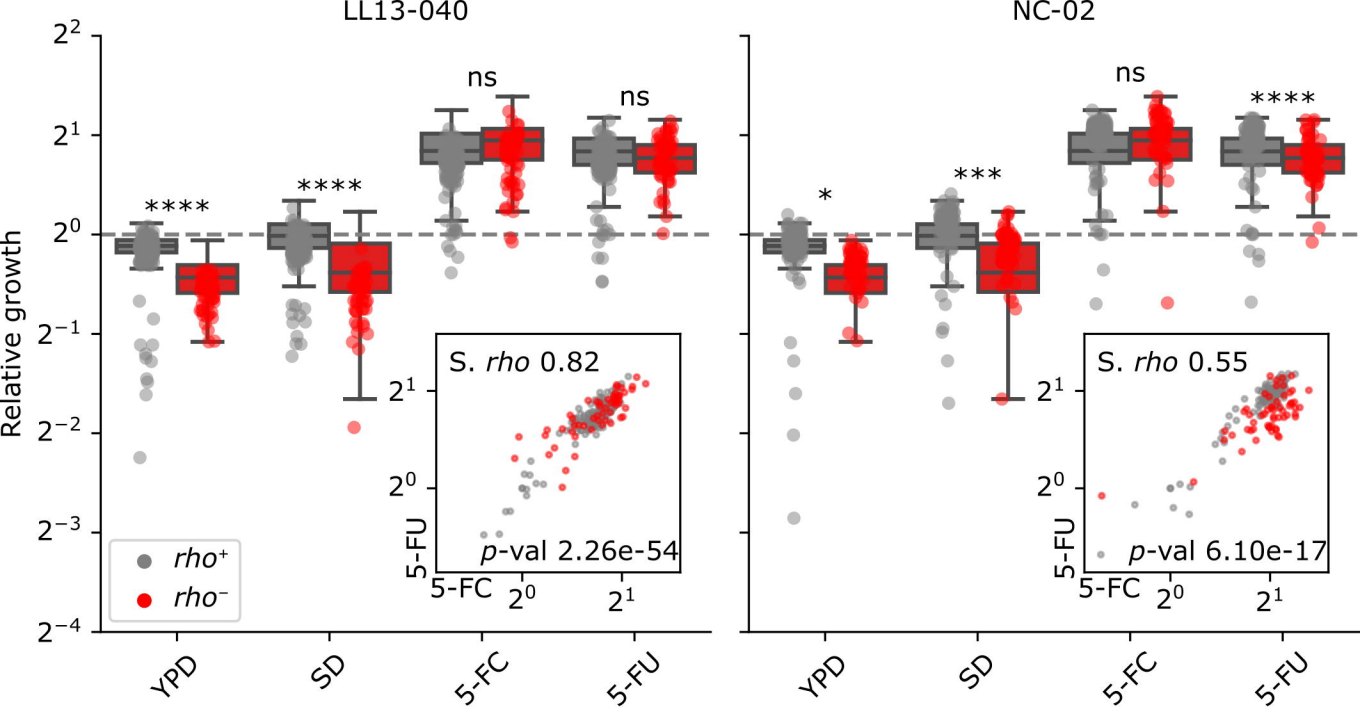
LL13-040
NC-02
Relative growth
2^2
2^1
2^0
2^{-1}
2^{-2}
2^{-3}
2^{-4}
****
****
ns
ns
*
***
ns
****
S. rho 0.82
p-val 2.26e-54
S. rho 0.55
p-val 6.10e-17
5-FU
5-FC
rho+
rho−
YPD
SD
5-FC
5-FU

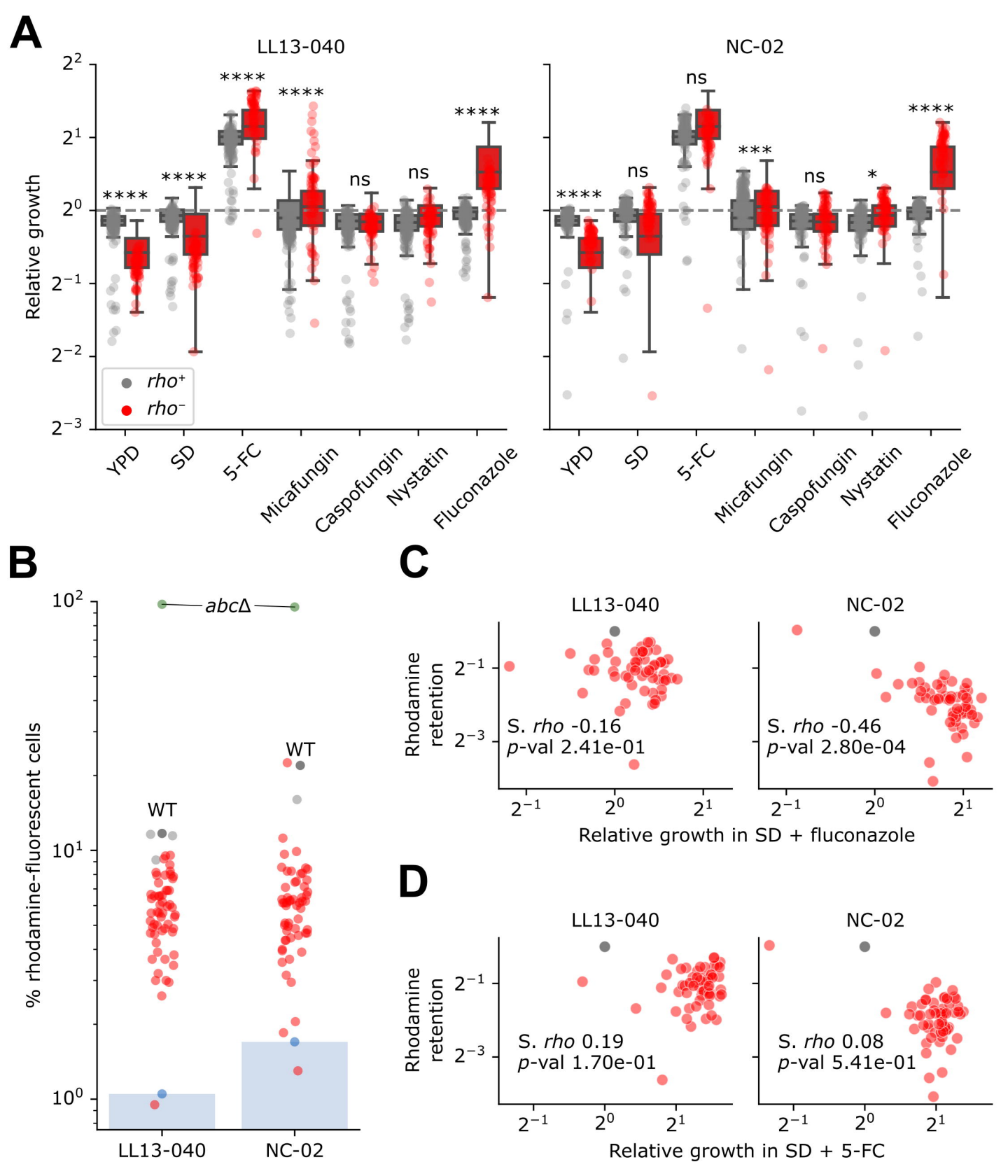
A
LL13-040
NC-02
Relative growth
rho+
rho−
YPD
SD
5-FC
Micafungin
Caspofungin
Nystatin
Fluconazole
B
abcΔ
WT
% rhodamine-fluorescent cells
C
Rhodamine retention
S. rho -0.16
p-val 2.41e-01
S. rho -0.46
p-val 2.80e-04
Relative growth in SD + fluconazole
D
S. rho 0.19
p-val 1.70e-01
S. rho 0.08
p-val 5.41e-01
Relative growth in SD + 5-FC

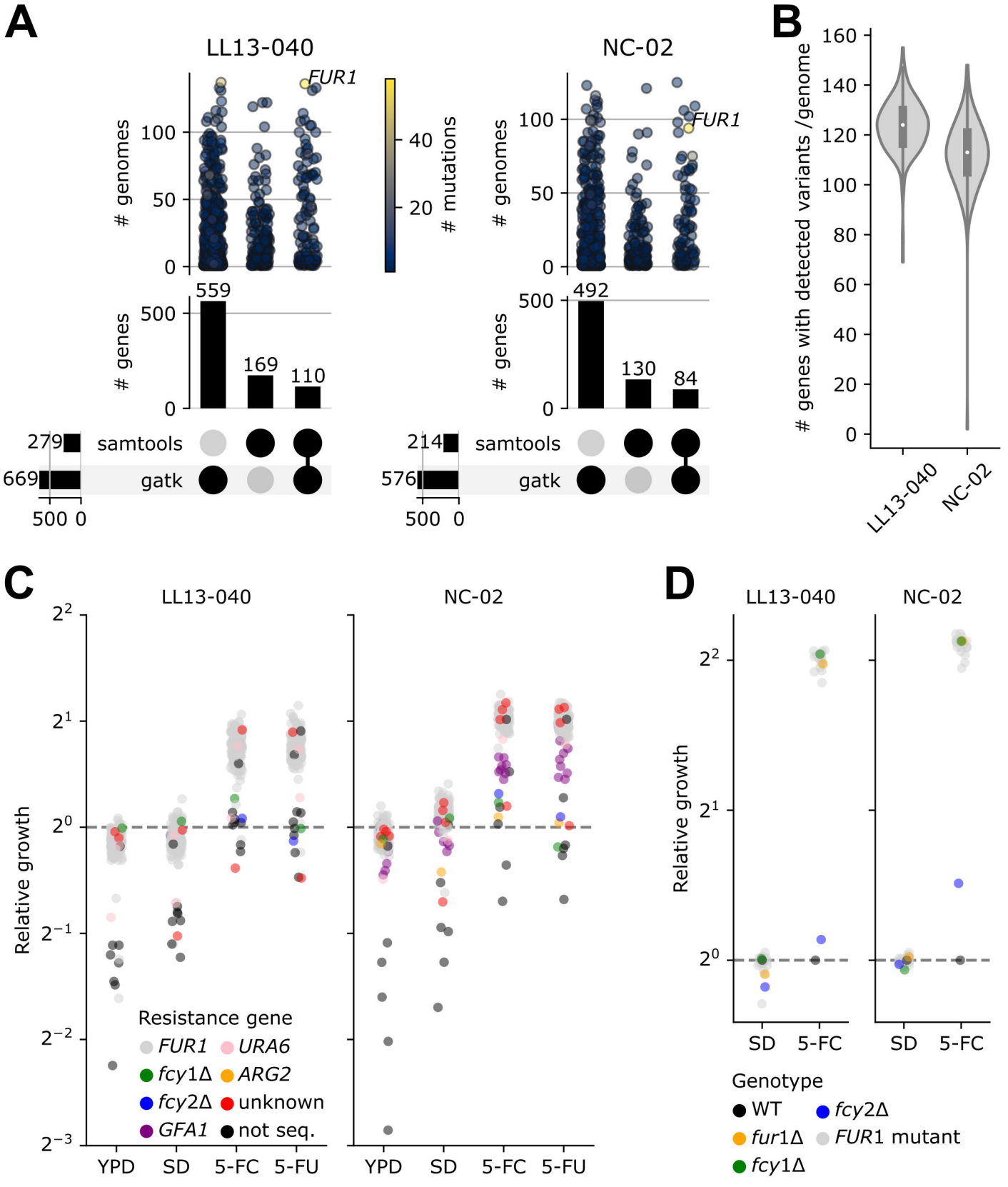
A
LL13-040
NC-02
FUR1
genomes
mutations
genes
559
169
110
492
130
84
279
669
214
576
samtools
gatk
500 0
B
genes with detected variants /genome
LL13-040
NC-02
C
Relative growth
Resistance gene
FUR1
URA6
fcy1Δ
ARG2
fcy2Δ
unknown
GFA1
not seq.
YPD
SD
5-FC
5-FU
D
Genotype
WT
fcy2Δ
fur1Δ
FUR1 mutant
fcy1Δ

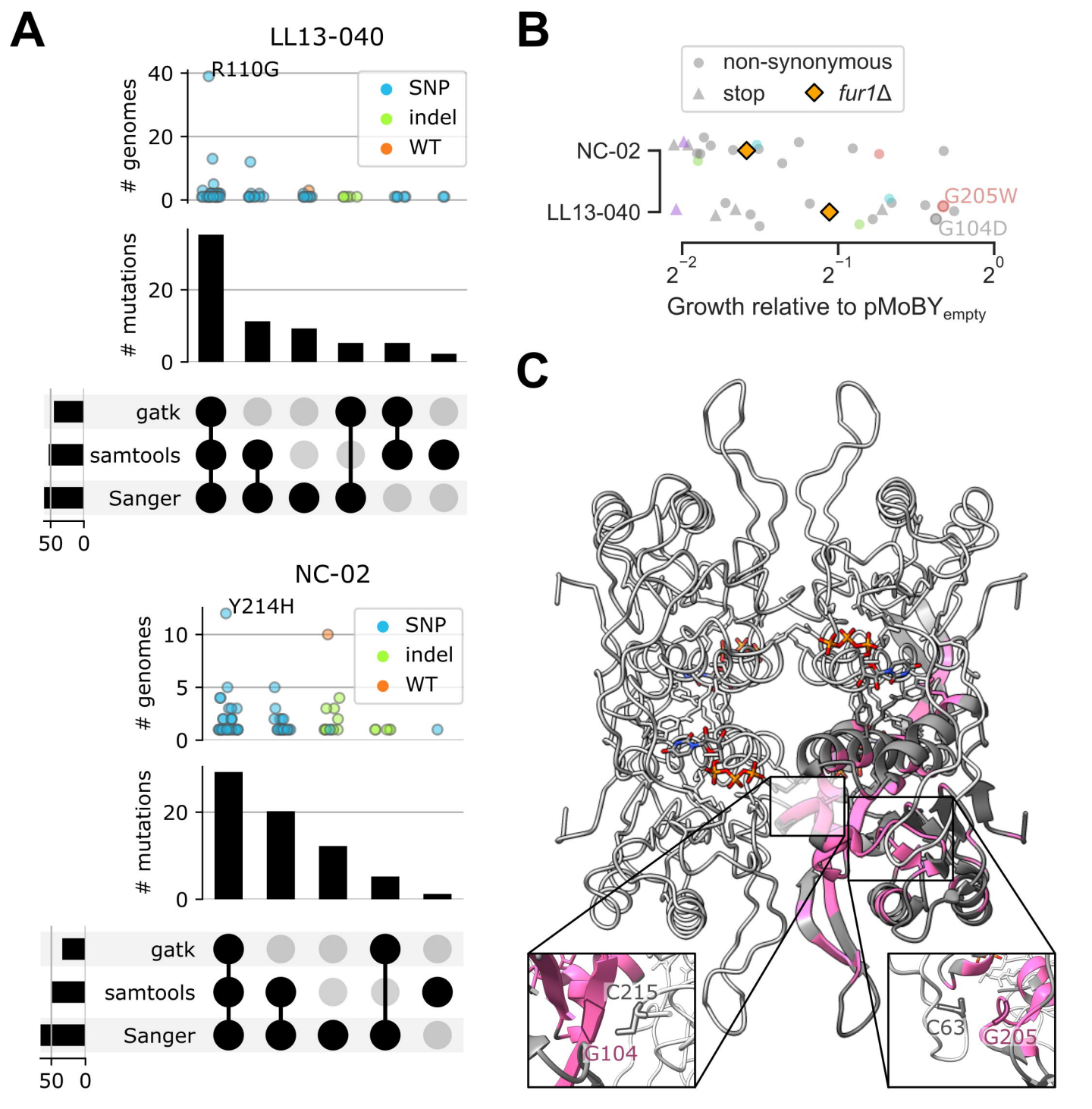
A
LL13-040
R110G
genomes
SNP
indel
WT
mutations
gatk
samtools
Sanger
NC-02
Y214H
B
non-synonymous
stop
fur1Δ
NC-02
LL13-040
G205W
G104D
Growth relative to pMoBY$_{empty}$
C
C215
G104
C63
G205

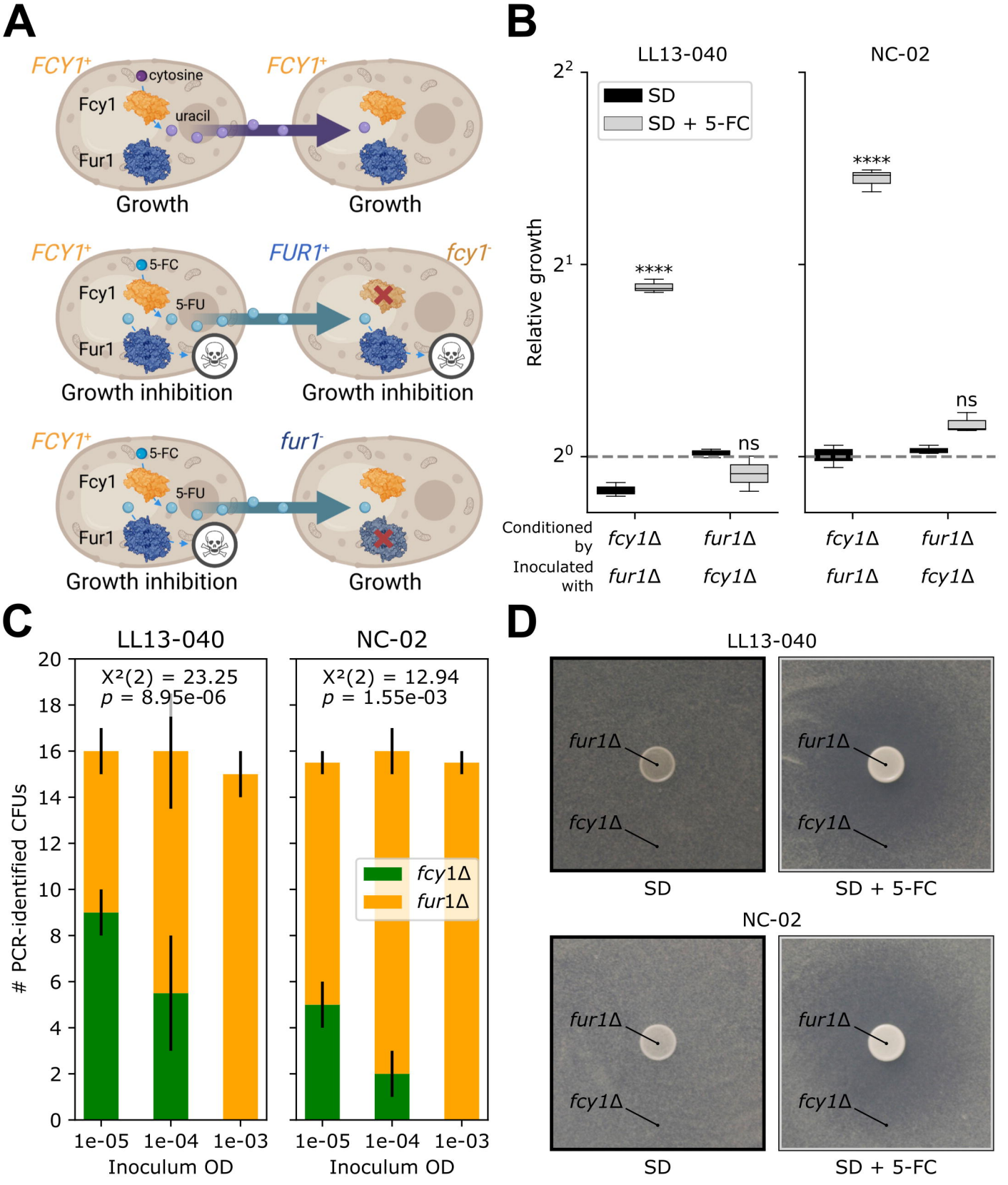
A
FCY1+
cytosine
Fcy1
uracil
Fur1
Growth
FCY1+
Growth
FCY1+
5-FC
Fcy1
5-FU
Fur1
Growth inhibition
FUR1+
fcy1-
Growth inhibition
FCY1+
5-FC
Fcy1
5-FU
Fur1
Growth inhibition
fur1-
Growth
B
LL13-040
NC-02
SD
SD + 5-FC
Relative growth
2^2
2^1
2^0
****
****
ns
ns
Conditioned by
Inoculated with
fcy1Δ
fur1Δ
fur1Δ
fcy1Δ
fcy1Δ
fur1Δ
fur1Δ
fcy1Δ
C
LL13-040
NC-02
X²(2) = 23.25
p = 8.95e-06
X²(2) = 12.94
p = 1.55e-03
# PCR-identified CFUs
fcy1Δ
fur1Δ
1e-05
1e-04
1e-03
Inoculum OD
D
LL13-040
fur1Δ
fcy1Δ
SD
SD + 5-FC
NC-02
SD
SD + 5-FC